The Flexibility of Long Chain Substituents Influences Spin-Crossover in Isomorphous Lipid Bilayer Crystals

Iurii Galadzhun[a], Rafal Kulmaczewski[a], Namrah Shahid[a], Oscar Cespedes,[b] Mark J. Howard[a] and Malcolm A. Halcrow[a,*]

[a]*School of Chemistry, University of Leeds, Leeds, UK LS2 9JT.*
E-mail: m.a.halcrow@leeds.ac.uk

[b]*School of Physics and Astronomy, University of Leeds, E. C. Stoner Building, Leeds, UK LS2 9JT*

Supporting Information

Experimental

Synthesis of 2-(4-iodopyrazol-1-yl)-6-(pyrazol-1-yl)pyridine. This was synthesised by an alternative to the literature procedure.[1] 4-Iodopyrazole (3.2 g, 16.7 mmol) was dissolved in a dmf (17 cm^3):thf (5 cm^3) solvent mixture. Solid NaH (60 % dispersion in mineral oil; 0.70 g, 17.5 mmol) was slowly added, and the reaction was stirred at room temperature until hydrogen evolution ceased. Solid 2-fluoro-6-(pyrazol-1-yl)pyridine[2] (2.7 g, 16.7 mmol) was then added, and the reaction mixture was stirred for 16 h at room temperature. Water (200 cm^3) was poured into the reaction mixture and the resultant white precipitate was collected, washed with hexane and dried *in vacuo*. The product was analysed without further purification. Yield 4.8 g, 86 %. Mp 141-142 °C. Found C 39.3, H 2.35, N 20.7 %. Calcd for C$_{11}$H$_8$IN$_5$ C 39.2, H 2.39, N 20.8 %. HR-ESI MS *m/z* 337.9892 (calcd for [(C$_{11}$H$_8$IN$_5$)H]$^+$ 337.9897), 359.9712 (calcd for [(C$_{11}$H$_8$IN$_5$)Na]$^+$ 359.9717). ^{1}H NMR (CDCl$_3$) δ 6.50 (dd, 1H, PzH H^4), 7.73 (s, 1H, PzI H^3), 7.76 (d, 1H, PzH H^3), 7.79 (dd, 1H, Py H^3), 7.89 (dd, 1H, Py H^5), 7.94 (dd, 1H, Py H^4), 8.55 (d, 1H, PzH H^5), 8.61 (s, 1H, PzI H^5). ^{13}C NMR (CDCl$_3$) δ 66.2 (PzI C^4), 108.3 (PzH C^4), 109.0 (Py C^3), 110.1 (Py C^5), 127.2 (PzH C^5), 131.7 (PzI C^5), 141.7 (Py C^4), 142.7 (PzH C^3), 147.2 (PzI C^3), 149.3, 150.2 (Py C^2 and C^6).

Synthesis of 2-(4-{dodec-1-ynyl}pyrazol-1-yl)-6-(pyrazol-1-yl)pyridine (L^1C_{12}). A mixture of 2-(4-iodopyrazol-1-yl)-6-(pyrazol-1-yl)pyridine (1.2 g, 3.56 mmol), [Pd(PPh$_3$)$_4$] (0.12 g, 0.1 mmol), triphenylphosphine (0.15 g, 0.56 mmol), CuI (0.15 g, 0.78 mmol), triethylamine (15 cm^3) and anhydrous dioxane (7 cm^3) was stirred in a Schlenk tube under N$_2$ for 2 hr. 1-Dodecyne (0.89 g, 5.34 mmol) was then added, and the mixture was stirred at 80˚C for 2 days. The cooled solution was filtered, and the filtrate was evaporated to dryness. Recrystallisation of the solid residue from from MeCN afforded the product as a white powder. Yield 0.64 g, 48 %. Mp 58-59 °C. Found C 73.6, H 7.75, N 18.5 %. Calcd for C$_{23}$H$_{29}$N$_5$ C 73.6, H 7.78, N 18.7 %. HR-ESI MS *m/z* 376.2493 (calcd for [(C$_{23}$H$_{29}$N$_5$)H]$^+$ 376.2496), 398.2319 (calcd for [(C$_{23}$H$_{29}$N$_5$)Na]$^+$ 398.2315), 773.4737 (calcd for [(C$_{23}$H$_{29}$N$_5$)$_2$Na]$^+$ 773.4738). ^{1}H NMR (CDCl$_3$) δ 0.88 (t, 3H, Ak C$^{12}H_3$), 1.28 (br s, 12H, Ak C$^6H_2$-C$^{11}H_2$), 1.45 (t, 2H, Ak C$^5H_2$), 1.61 (t, 2H, Ak C$^4H_2$), 2.41 (t, 2H, Ak C$^3H_2$), 6.50 (dd, 1H, PzH H^4), 7.75 (s, 1H, PzAk H^3), 7.77 (d, 1H, PzH H^3), 7.82 (dd, 1H, Py H^5), 7.87 (dd, 1 H, Py H^3), 7.93 (t, 1H, Py H^4), 8.55 (d, 1H, PzH H^5), 8.59 (s, 1H, PzAk H^5). ^{13}C NMR (CDCl$_3$) δ 14.3 (1C, Ak C^{12}), 19.7 (1C, Ak C^3), 22.8, 29.1, 29.3, 29.5, 29.7, 29.7, 32.1 (all 1C, Ak C^5- C^{11}), 28.9 (1C, Ak C^4), 70.9 (1C, PzAk C^4), 92.8 (1C, Ak C^2), 106.6 (1C, Ak C^1), 108.2 (1C, PzH C^4), 109.5 (1C, Py C^5), 109.8 (1C, Py C^3), 127.1 (1C, PzH C^3), 129.1 (1C, PzAk C^3), 141.6 (1C, Py C^4), 142.6 (1C, PzH C^5), 144.7 (1C, PzAk C^5), 149.7, 150.2 (both 1C, Py C^2 and C^6).

Synthesis of 2-(4-{tetradec-1-ynyl}pyrazol-1-yl)-6-(pyrazol-1-yl)pyridine (L^1C_{14}). Method as for L^1C_{12}, using the following quantities: 2-(4-iodopyrazol-1-yl)-6-(pyrazol-1-yl)pyridine (1.45 g, 4.3 mmol), [Pd(PPh$_3$)$_4$] (0.15 g, 0.13 mmol), triphenylphosphine (0.18 g, 0.69 mmol), CuI (0.18 g, 0.95 mmol), triethylamine (18 cm^3), dioxane (9 cm^3) and 1-tetradecyne (1.25 g, 6.4 mmol). The product was obtained as colourless crystals following recrystallisation from acetonitrile. Yield 0.64 g, 48 %. Mp 65-66 °C. Found C 74.2, H 7.92, N 17.0 %. Calcd for C$_{25}$H$_{33}$N$_5$ C 74.4, H 8.24, N 17.4 %. HR-ESI MS *m/z* 404.2809 (calcd for [(C$_{25}$H$_{33}$N$_5$)H]$^+$ 408.2803), 426.2628 (calcd for [(C$_{25}$H$_{33}$N$_5$)Na]$^+$ 426.2628), 829.5364 (calcd for [(C$_{25}$H$_{33}$N$_5$)$_2$Na]$^+$ 829.5364). ^{1}H NMR (CDCl$_3$) δ 0.87 (t, 3H, Ak C$^{14}H_3$), 1.26 (br s, 16H, Ak C$^6H_2$-C$^{13}H_2$), 1.45 (t, 2H, Ak C$^5H_2$), 1.61 (t, 2H, Ak C$^4H_2$), 2.41 (t, 2H, Ak C$^3H_2$), 6.49 (dd, 1H, PzH H^4), 7.75 (s, 1H, PzAk H^3), 7.77 (d, 1H, PzH H^3), 7.82 (dd, 1H, Py H^5), 7.87 (dd, 1H, Py H^3), 7.93 (t, 1H, Py H^4), 8.55 (d, 1H, PzH H^5), 8.59 (s, 1H, PzAk H^5). ^{13}C NMR (CDCl$_3$) δ 14.3 (1C, Ak C^{14}), 19.7 (1C, Ak C^3), 22.8 (1C), 29.1 (1C), 29.3 (1C), 29.5 (1C), 29.7 (1C), 29.8 (2C), 29.8 (1C), 32.1 (1C; Ak C^5-C^{13}), 28.9 (1C, Ak C^4), 70.9 (1C, PzAk C^4), 92.8 (1C, Ak C^2), 106.6 (1C, Ak C^1), 108.2 (1C, PzH C^4), 109.5 (1C, Py C^5), 109.8 (1C, Py C^3), 127.1 (1C, PzH C^3), 129.1 (1C, PzAk C^3), 141.6 (1C, Py C^4), 142.6 (1C, PzH C^5), 144.7 (1C, PzAk C^5), 149.6, 150.2 (both 1C, Py C^2 and C^6).

Synthesis of 2-(4-{hexadec-1-ynyl}pyrazol-1-yl)-6-(pyrazol-1-yl)pyridine (L^1C_{16}). Method as for L^1C_{12}, using the following quantities: 2-(4-iodopyrazol-1-yl)-6-(pyrazol-1-yl)pyridine (1.45 g, 4.3 mmol), [Pd(PPh$_3$)$_4$] (0.15 g, 0.13 mmol), triphenylphosphine (0.18 g, 0.69 mmol), CuI (0.18 g, 0.95 mmol), triethylamine (18 cm^3), dioxane (9 cm^3) and 1-hexadecyne (1.43 g, 6.44 mmol). The product was a white polycrystalline solid. Yield 0.78 g, 42 %. Mp 69-71 °C. Found C 75.1, H 8.83, N 16.0 %. Calcd for C$_{27}$H$_{37}$N$_5$ C 75.1, H 8.64, N 16.2 %. HR-ESI MS m/z 432.3122 (calcd for [(C$_{27}$H$_{37}$N$_5$)H]$^+$ 432.3122), 454.2936 (calcd for [(C$_{27}$H$_{37}$N$_5$)Na]$^+$ 454.2941), 885.5986 (calcd for [(C$_{27}$H$_{37}$N$_5$)$_2$Na]$^+$ 885.5990). ^{1}H NMR (CDCl$_3$) δ 0.88 (t, 3H, Ak C$^{14}H_3$), 1.28 (br s, 20H, Ak C$^6H_2$-C$^{13}H_2$), 1.45 (t, 2H, Ak C$^5H_2$), 1.59 (t, 2H, Ak C$^4H_2$), 2.41 (t, 2H, Ak C$^3H_2$), 6.50 (dd, 1H, PzH H^4), 7.75 (s, 1H, PzAk H^3), 7.77 (d, 1H, PzH H^3), 7.82 (dd, 1H, Py H^5), 7.87 (dd, 1H, Py H^3), 7.93 (t, 1H, Py H^4), 8.55 (d, 1H, PzH H^5), 8.59 (s, 1H, PzAk H^5). ^{13}C NMR (CDCl$_3$) δ 14.3 (1C, Ak C^{16}), 19.7 (1C, Ak C^3), 22.8 (1C), 29.1 (1C), 29.3 (1C), 29.5 (1C), 29.7 (1C), 29.8 (3C), 29.8 (2C), 32.1 (1C; Ak C^5-C^{15}), 28.9 (1C, Ak C^4), 70.9 (1C, PzAk C^4), 92.8 (1C, Ak C^2), 106.6 (1C, Ak C^1), 108.2 (1C, PzH C^4), 109.5 (1C, Py C^5), 109.8 (1C, Py C^3), 127.1 (1C, PzH C^3), 129.1 (1C, PzAk C^3), 141.6 (1C, Py C^4), 142.6 (1C, PzH C^5), 144.7 (1C, PzAk C^5), 149.7, 150.2 (both 1C, Py C^2 and C^6).

Synthesis of 2-(4-{octadec-1-ynyl}pyrazol-1-yl)-6-(pyrazol-1-yl)pyridine (L^1C_{18}). Method as for L^1C_{12}, using the following quantities: 2-(4-iodopyrazol-1-yl)-6-(pyrazol-1-yl)pyridine (1.02 g, 3.0 mmol), [Pd(PPh$_3$)$_4$] (0.11 g, 0.091 mmol), triphenylphosphine (0.13 g, 0.48 mmol), CuI (0.13 g, 0.67 mmol), triethylamine (12 cm^3), dioxane (6 cm^3) and 1-octadecyne (0.76 g, 3.0 mmol). The product was a white polycrystalline solid. Yield 0.57 g, 34 %. Mp 75-76 °C. Found C 75.6, H 8.74, N 15.0 %. Calcd for C$_{29}$H$_{41}$N$_5$ C 75.8; H 8.99; N 15.2 %. HR-ESI MS m/z 460.3429 (calcd for [(C$_{29}$H$_{41}$N$_5$)H]$^+$ 460.3435), 482.3250 (calcd for [(C$_{29}$H$_{41}$N$_5$)Na]$^+$ 482.3254). ^{1}H NMR (CDCl$_3$) δ 0.88 (t, 3H, Ak C$^{18}H_3$), 1.25 (br s, 24H, Ak C$^6H_2$-C$^{17}H_2$), 1.45 (t, 2H, Ak C$^5H_2$), 1.61 (t, 2H, Ak C$^4H_2$), 2.41 (t, 2H, Ak C$^3H_2$), 6.50 (dd, 1H, PzH H^4), 7.75 (s, 1H, PzAk H^3), 7.76 (d, 1H, PzH H^3), 7.82 (dd, 1H, Py H^5), 7.87 (dd, 1H, Py H^3), 7.93 (t, 1H, Py H^4), 8.56 (d, 1H, PzH H^5), 8.60 (s, 1H, PzAk H^5). ^{13}C NMR (CDCl$_3$) δ 14.3 (1C, Ak C^{18}), 19.7 (1C, Ak C^3), 22.8 (1C), 29.1 (1C), 29.3 (2C), 29.5 (2C), 29.8 (6C), 32.1 (1C; Ak C^5-C^{17}), 28.9 (1C, Ak C^4), 70.8 (1C, PzAk C^4), 92.8 (1C, Ak C^2), 106.6 (1C, Ak C^1), 108.2 (1C, PzH C^4), 109.5 (1C, Py C^5), 109.8 (1C, Py C^3), 127.1 (1C, PzH C^3), 129.1 (1C, PzAk C^3), 141.6 (1C, Py C^4), 142.6 (1C, PzH C^5), 144.7 (1C, PzAk C^5), 149.6, 150.2 (both 1C, Py C^2 and C^6).

Synthesis of 2-(4-dodecylpyrazol-1-yl)-6-(pyrazol-1-yl)pyridine (L^2C_{12}). A solution of L^1C_{12} (0.35 g, 0.93 mmol) in ethyl acetate (150 cm^3) was degassed in a Schlenk tube. Solid 10% Pd on activated carbon (0.27 g, 0.23 mmol) was then added, and the solution was placed under an atmosphere of H$_2$. The mixture was stirred at room temperature for 4 days, while being monitored by thin layer chromatography. The resultant solution was filtered through a celite plug, and the celite was washed with more ethyl acetate (120 cm^3). Evaporation of the combined organic fractions to dryness yielded the product as a white powder, which was analysed without further purification. Yield 0.32 g, 91%. Mp 66-67 °C. Found C 72.7, H 8.80, N 18.3 %. Calcd for C$_{23}$H$_{33}$N$_5$ C 72.8, H 8.76, N 18.5 %. HR-ESI MS m/z 380.2812 (calcd for [(C$_{23}$H$_{33}$N$_5$)H]$^+$ 380.2809), 402.2632 (calcd for [(C$_{23}$H$_{33}$N$_5$)Na]$^+$ 402.2628), 781.5367 (calcd for [(C$_{23}$H$_{33}$N$_5$)$_2$Na]$^+$ 781.5364). ^{1}H NMR (CDCl$_3$) δ 0.88 (t, 3H, Ak C$^{12}H_3$), 1.26 (br s, 16H, Ak C$^4H_2$-C$^{11}H_2$), 1.35 (br t, 2H, Ak C$^3H_2$), 1.64 (t, 2H, Ak C$^2H_2$), 2.55 (t, 2H, Ak C$^1H_2$), 6.50 (dd, 1H, PzH H^4), 7.59 (s, 1H, PzAk H^3), 7.76 (br d, 1H, Py H^3), 7.80 (d, 1H, PzH H^3), 7.82 (d, 1H, Py H^5), 7.90 (t, 1H, Py H^4), 8.32 (s, 1H, PzAk H^5), 8.59 (d, 1H, PzH H^5). ^{13}C NMR (CDCl$_3$) δ 14.3 (1C, Ak C^{12}), 22.8 (1C), 29.4 (1C), 29.5 (1C), 29.6 (1C), 29.8 (1C), 29.8 (2C), 32.1 (1C; Ak C^4-C^{11}), 24.4 (1C, Ak C^1), 29.8 (1C, Ak C^3), 30.8 (1C, Ak C^2), 108.0 (1C, PzH C^4), 109.0 (1C, Py C^3), 109.2 (1C, Py C^5), 124.6 (1C, PzAk C^4), 124.9 (1C, PzAk C^3), 127.2 (1C, PzH C^3), 141.4 (1C, Py C^4), 142.5 (1C, PzH C^5), 142.8 (1C, PzAk C^5), 150.1, 150.3 (both 1C, Py C^2 and C^6).

Synthesis of 2-(4-tetradecylpyrazol-1-yl)-6-(pyrazol-1-yl)pyridine (L^2C_{14}). Method as for L^2C_{12}, using the following quantities: L^1C_{14} (0.40 g, 0.99 mmol), ethyl acetate (160 cm^3) and 10% Pd on activated carbon (0.29 g, 0.25 mmol). Yield 0.22 g, 54 %. Mp 72-73 °C. Found C 73.8, H 9.27, N 17.1

%. Calcd for $C_{25}H_{37}N_5$ C 73.7, H 9.15, N 17.2 %. HR-ESI MS m/z 408.3124 (calcd for $[(C_{25}H_{37}N_5)H]^+$ 408.3122), 454.2943 (calcd for $[(C_{25}H_{37}N_5)Na]^+$ 454.2941), 837.5991 (calcd for $[(C_{25}H_{37}N_5)_2Na]^+$ 837.5990). ^1H NMR (CDCl$_3$) δ 0.88 (t, 3H, Ak C$^{14}H_3$), 1.26 (br s, 20H, Ak C$^4H_2$-C$^{13}H_2$), 1.35 (br t, 2H, Ak C$^3H_2$), 1.64 (t, 2H, Ak C$^2H_2$), 2.55 (t, 2H, Ak C$^1H_2$), 6.49 (dd, 1H, PzH H^4), 7.59 (s, 1H, PzAk H^3), 7.76 (br d, 1H, Py H^3), 7.80 (d, 1H, PzH H^3), 7.82 (d, 1H, Py H^5), 7.90 (t, 1H, Py H^4), 8.32 (s, 1H, PzAk H^5), 8.59 (d, 1H, PzH H^5). ^{13}C NMR (CDCl$_3$) δ 14.3 (1C, Ak C^{14}), 22.8 (1C), 29.4 (1C), 29.5 (1C), 29.6 (1C), 29.8 (1C), 29.8 (4C), 32.1 (1C; Ak C^4-C^{13}), 24.4 (1C, Ak C^1), 29.8 (1C, Ak C^3), 30.8 (1C, Ak C^2), 108.0 (1C, PzH C^4), 109.0 (1C, Py C^3), 109.2 (1C, Py C^5), 124.6 (1C, PzAk C^4), 124.9 (1C, PzAk C^3), 127.2 (1C, PzH C^3), 141.4 (1C, Py C^4), 142.5 (1C, PzH C^5), 142.8 (1C, PzAk C^5), 150.1, 150.3 (both 1C, Py C^2 and C^6).

Synthesis of 2-(4-hexadecylpyrazol-1-yl)-6-(pyrazol-1-yl)pyridine (L^2C_{16}). Method as for L^2C_{12}, using the following quantities: L^1C_{16} (0.40 g, 0.93 mmol), ethyl acetate (150 cm^3) and 10% Pd on activated carbon (0.27 g, 0.23 mmol). Yield 0.38 g, 94 %. Mp 78-79 $^\circ$C. Found C 74.5, H 9.57, N 15.9 %. Calcd for $C_{27}H_{41}N_5$ C 74.4, H 9.49, N 16.1 %. HR-ESI MS m/z 436.3438 (calcd for $[(C_{27}H_{41}N_5)H]^+$ 436.3435), 458.3258 (calcd for $[(C_{27}H_{41}N_5)Na]^+$ 458.3254), 893.6620 (calcd for $[(C_{27}H_{41}N_5)_2Na]^+$ 893.6616). ^1H NMR (CDCl$_3$) δ 0.88 (t, 3H, Ak C$^{14}H_3$), 1.25 (br s, 24H, Ak C$^4H_2$-C$^{13}H_2$), 1.35 (br t, 2H, Ak C$^3H_2$), 1.64 (t, 2H, Ak C$^2H_2$), 2.54 (t, 2H, Ak C$^1H_2$), 6.48 (pseudo-t, 1H, PzH H^4), 7.58 (s, 1H, PzAk H^3), 7.75 (br s, 1H, Py H^3), 7.80 (d, 1H, Py H^5), 7.81 (br s, 1H, PzH H^3), 7.89 (pseudo-t, 1H, Py H^4), 8.31 (s, 1H, PzAk H^5), 8.58 (d, 1H, PzH H^5). ^{13}C NMR (CDCl$_3$) δ 14.2 (1C, Ak C^{16}), 22.8 (1C), 29.4 (1C), 29.5 (1C), 29.6 (1C), 29.8 (7C), 32.1 (1C; Ak C^4-C^{15}), 24.4 (1C, Ak C^1), 29.8 (1C, Ak C^3), 30.8 (1C, Ak C^2), 108.0 (1C, PzH C^4), 108.9 (1C, Py C^3), 109.1 (1C, Py C^5), 124.6 (1C, PzAk C^4), 124.8 (1C, PzAk C^3), 127.1 (1C, PzH C^3), 141.4 (1C, Py C^4), 142.4 (1C, PzH C^5), 142.7 (1C, PzAk C^5), 150.1, 150.3 (both 1C, Py C^2 and C^6).

Synthesis of 2-(4-octadecylpyrazol-1-yl)-6-(pyrazol-1-yl)pyridine (L^2C_{18}). Method as for L^2C_{12}, using the following quantities: L^1C_{18} (0.24 g, 0.45 mmol), ethyl acetate (75 cm^3) and 10% Pd on activated carbon (0.13 g, 0.11 mmol). Yield 0.22 g, 91 %. Mp 81-82 $^\circ$C. Found C 75.1, H 9.56, N 14.9 %. Calcd for $C_{29}H_{45}N_5$ C 75.1; H 9.78; N 15.1 %. HR-ESI MS m/z 464.3752 (calcd for $[(C_{29}H_{45}N_5)H]^+$ 464.3748), 486.3570 (calcd for $[(C_{29}H_{45}N_5)Na]^+$ 486.3567). ^1H NMR (CDCl$_3$) δ 0.88 (t, 3H, Ak C$^{14}H_3$), 1.25 (br s, 28H, Ak C$^4H_2$-C$^{13}H_2$), 1.34 (br t, 2H, Ak C$^3H_2$), 1.63 (t, 2H, Ak C$^2H_2$), 2.55 (t, 2H, Ak C$^1H_2$), 6.50 (pseudo-t, 1H, PzH H^4), 7.59 (s, 1H, PzAk H^3), 7.80 (br s, 1H, Py H^3), 7.82 (d, 1H, Py H^5), 7.91 (dd, 1H, PzH H^3), 7.91 (pseudo-t, 1H, Py H^4), 8.32 (s, 1H, PzAk H^5), 8.59 (d, 1H, PzH H^5). ^{13}C NMR (CDCl$_3$) δ 14.3 (1C, Ak C^{18}), 22.9 (1C), 29.4 (1C), 29.5 (1C), 29.6 (1C), 29.9 (9C), 32.1 (1C; Ak C^4-C^{17}), 24.4 (1C, Ak C^1), 29.8 (1C, Ak C^3), 30.8 (1C, Ak C^2), 108.0 (1C, PzH C^4), 109.0 (1C, Py C^3), 109.1 (1C, Py C^5), 124.6 (1C, PzAk C^4), 124.9 (1C, PzAk C^3), 127.2 (1C, PzH C^3), 141.4 (1C, Py C^4), 142.5 (1C, PzH C^5), 142.8 (1C, PzAk C^5), 150.1, 150.3 (both 1C, Py C^2 and C^6).

Synthesis of the Iron Complexes. Two procedures were followed for the preparation of the complexes, according to the solubilities of the reactants and products. In both cases, the products were recrystallised from 1,2-dichloroethane/pentane if further purification was required. Crystallised yields were in the range of 20−80%, depending on the solubility of the complex.

Procedure A: the appropriate ligand (0.37 mmol) and Fe[BF$_4$]$_2$·6H$_2$O (0.070 g, 0.19 mmol) were stirred in dichloromethane (10 cm^3) until all the solid had dissolved. Slow diffusion of di-*iso*propylether into the filtered solution yielded the products as an orange or yellow powder, which was collected and washed with pentane before drying.

Procedure B: Solutions of the appropriate ligand (0.37 mmol) in 1,2-dichloroethane (5 cm^3), and of Fe[BF$_4$]$_2$·6H$_2$O (0.070 g, 0.19 mmol) in acetone (10 cm^3) were mixed and briefly stirred at room temperature. The orange solution was then concentrated to *ca.* 50 % of its original volume and filtered. Slow diffusion of *n*-pentane into the solution yielded the complex as an orange or yellow solid, which was collected and washed with pentane before drying.

Since we did not obtain [Fe(L^{1}C$_{18}$)$_2$][BF$_4$]$_2$ in analytical purity, this compound is not discussed further in the paper.

For [Fe(L^{1}C$_{12}$)$_2$][BF$_4$]$_2$. Procedure A. Found C 56.2, H 6.12, N 14.2 %. Calcd for C$_{46}$H$_{58}$B$_2$F$_8$FeN$_{10}$ C 56.4, H 5.96, N 14.3 %. ^{1}H NMR (CDCl$_3$) δ −1.7 (2H, Py H^4), 1.0 (6H, Ak $C^{12}H_3$), 1.4 (28H, C^5H_2-$C^{11}H_2$), 4.4 (4H, Ak C^4H_2), 11.2 (4H, Ak C^3H_2), 28.9, 37.2, 41.1 (all 2H, Py H^3 and H^5 + PzAk H^5), 51.0 (2H, PzH H^5), 58.8, 60.8, 67.8 (all 2H, PzH H^3 and H^4 + PzAk H^3).

For [Fe(L^{1}C$_{14}$)$_2$][BF$_4$]$_2$. Procedure A. Found C 56.9, H 6.62, N 13.1 %. Calcd for C$_{50}$H$_{66}$B$_2$F$_8$FeN$_{10}$·H$_2$O C 56.9; H 6.50; N 13.3 %. ^{1}H NMR (CDCl$_3$) δ −1.8 (2H, Py H^4), 0.9 (6H, Ak $C^{14}H_3$), 1.4 (36H, C^5H_2-$C^{13}H_2$), 4.4 (4H, Ak C^4H_2), 11.7 (4H, Ak C^3H_2), 28.9, 37.1, 41.0 (all 2H, Py H^3 and H^5 + PzAk H^5), 51.2 (2H, PzH H^5), 58.6, 60.7, 67.7 (all 2H, PzH H^3 and H^4 + PzAk H^3).

For [Fe(L^{1}C$_{16}$)$_2$][BF$_4$]$_2$. Procedure A. Found C 59.2 H 6.75, N 12.7 %. Calcd for C$_{54}$H$_{74}$B$_2$F$_8$FeN$_{10}$ C 59.4, H 6.83, N 12.8 %. ^{1}H NMR (CDCl$_3$) δ −1.7 (2H, Py H^4), 0.9 (6H, Ak $C^{16}H_3$), 1.4 (44H, C^5H_2-$C^{15}H_2$), 4.4 (4H, Ak C^4H_2), 10.9 (4H, Ak C^3H_2), 29.2, 37.1, 41.0 (all 2H, Py H^3 and H^5 + PzAk H^5), 50.9 (2H, PzH H^5), 58.7, 60.8, 67.7 (all 2H, PzH H^3 and H^4 + PzAk H^3).

For [Fe(L^{2}C$_{12}$)$_2$][BF$_4$]$_2$. Procedure B. Found C 54.5, H 6.72, N 13.9 %. Calcd for C$_{46}$H$_{66}$B$_2$F$_8$FeN$_{10}$·H$_2$O C 54.9, H 6.82, N 13.9 %. ^{1}H NMR (CD$_3$CN) δ 0.9 (6H, Ak $C^{12}H_3$), 1.3 (28H, C^5H_2-$C^{11}H_2$), 1.9 (4H, Ak C^4H_2), 3.0 (4H, Ak C^3H_2), 3.5 (2H, Py H^4), 6.0 (4H, Ak C^2H_2), 6.2 (4H, Ak C^1H_2), 33.0 (2H), 35.5 (3H), 35.9 (2H) (Py H^3 and H^5 + PzH H^5 + PzAk H^5), 54.7 (4H) and 58.8 (2H) (PzH H^3 and H^4 + PzAk H^3).

For [Fe(L^{2}C$_{14}$)$_2$][BF$_4$]$_2$. Procedure B. Found C 56.2, H 6.88, N 13.3 %. Calcd for C$_{50}$H$_{74}$B$_2$F$_8$FeN$_{10}$·H$_2$O C 56.5, H 7.21, N 13.2 %. ^{1}H NMR (CD$_3$CN) δ 0.9 (6H, Ak $C^{14}H_3$), 1.3 (36H, C^5H_2-$C^{13}H_2$), 1.9 (4H, Ak C^4H_2), 2.9 (4H, Ak C^3H_2), 3.4 (2H, Py H^4), 6.0 (4H, Ak C^2H_2), 6.3 (4H, Ak C^1H_2), 33.0 (2H), 35.4 (4H), 35.9 (2H) (Py H^3 and H^5 + PzH H^5 + PzAk H^5), 54.6 (4H) and 58.7 (2H) (PzH H^3 and H^4 + PzAk H^3).

For [Fe(L^{2}C$_{16}$)$_2$][BF$_4$]$_2$. Procedure B. Found C 58.8, H 7.37, N 12.6 %. Calcd for C$_{54}$H$_{82}$B$_2$F$_8$FeN$_{10}$ C 58.9, H 7.51, N 12.7 %. ^{1}H NMR (CD$_3$CN) δ 0.9 (6H, Ak $C^{16}H_3$), 1.3 (44H, C^5H_2-$C^{15}H_2$), 1.9 (4H, Ak C^4H_2), 3.0 (4H, Ak C^3H_2), 3.4 (2H, Py H^4), 5.9 (4H, Ak C^2H_2), 6.3 (4H, Ak C^1H_2), 33.0 (2H), 35.4 (4H), 35.9 (2H) (Py H^3 and H^5 + PzH H^5 + PzAk H^5), 54.5 (4H) and 58.6 (2H) (PzH H^3 and H^4 + PzAk H^3).

For [Fe(L^{2}C$_{18}$)$_2$][BF$_4$]$_2$. Procedure B. Found C 60.0, H 7.60, N 12.9 %. Calcd for C$_{58}$H$_{90}$B$_2$F$_8$FeN$_{10}$ C 60.2, H 7.84, N 12.1 %.

Single crystal X-ray structures

L^1C$_{12}$ was crystallised by slow evaporation of an acetonitrile solution, while small crystals of L^2C$_{12}$, L^2C$_{14}$ and [Fe(L^2C$_n$)$_2$][BF$_4$]$_2$ (n = 12, 16, 18) were grown by slow diffusion of pentane vapour into 1,2-dichloroethane solutions of those compounds. Experimental data for the crystal structures are listed in Tables S1 and S2 below.

Diffraction data for L^1C$_{12}$, L^2C$_{12}$, L^2C$_{14}$ and [Fe(L^2C$_{12}$)$_2$][BF$_4$]$_2$ were recorded at station I19 of the Diamond synchrotron (λ = 0.6889 Å). This was necessary owing to their weak diffraction, which is probably a consequence of their small crystal size. Datasets of [Fe(L^2C$_{16}$)$_2$][BF$_4$]$_2$ (Agilent Supernova diffractometer, Cu-K_α radiation) and [Fe(L^2C$_{18}$)$_2$][BF$_4$]$_2$ (synchrotron radiation) were also collected, which proved too weak for meaningful anisotropic structure refinements but confirmed the isomorphous nature of the [Fe(L^2C$_n$)$_2$][BF$_4$]$_2$ series.

Experimental details of the structure determinations are listed in Tables S1 and S2. The structures were all solved by direct methods (*SHELXS97*[3]), and developed by full least-squares refinement on F^2 (*SHELXL97*[3]). Crystallographic figures were prepared using *XSEED*,[4] and other structural indices tabulated in the Supporting Information were calculated with *Olex2*.[5]

Crystallographic refinements Unless otherwise stated, all crystallographically ordered non-H atoms in the structures described below were refined anisotropically, and H atoms were placed in calculated positions and refined using a riding model.

No disorder is present in any of the crystal structures in this study. All the H atoms in L^2C_{12} and L^2C_{14} were located in the Fourier map and refined positionally, with U_{iso} constrained to 1.5x U_{eq} of the corresponding C atom for methyl group H atoms, or to 1.2x $U_{eq}\{C\}$ for other H atoms. H atom positions were not refined for L^1C_{12} to preserve the lower data:parameter ratios in that refinement, or for $[Fe(L^2C_{12})_2][BF_4]_2$ because of the heavy atoms present in that structure.

While L^1C_{12} adopts a handed space group, its absolute structures could not be unambiguously determined owing to its light atom composition. Hence the Friedel opposite reflections in that dataset were merged for the final least squares cycles.

The asymmetric unit of $[Fe(L^2C_{12})_2][BF_4]_2$ contains two formula units of the compound: that is, two crystallographically unique complex dications and four BF_4^- anions. No disorder is present in the model, and no restraints were applied to the refinement.

Other measurements

Elemental microanalyses were performed by the microanalytical services at the London Metropolitan University School of Human Sciences. Electrospray mass spectra were recorded on a Bruker MicroTOF-q instrument from $CHCl_3$ solution. Diamagnetic NMR spectra employed a Bruker AV3HD spectrometer operating at 400.1 MHz (^{1}H) or 100.6 MHz (^{13}C), while paramagnetic ^{1}H NMR spectra were obtained with a Bruker AV3 spectrometer operating at 300.1 MHz. Thermogravimetric analyses employed a TA Instruments TGA Q50 analyser with a temperature ramp of 10 K min^{-1} under a stream of nitrogen gas. Differential scanning calorimetry (DSC) measurements used a TA Instruments DSC Q20 calorimeter, heating at a rate of 10 K min^{-1}. X-ray powder diffraction measurements were obtained at room temperature from a Bruker D2 Phaser diffractometer, using Cu-K_α radiation ($\lambda = 1.5419$ Å).

Solid state magnetic susceptibility measurements were performed using Quantum Design SQUID or VSM SQUID magnetometers, in an applied field of 5000 G with a temperature ramp of 5 K min^{-1}. Diamagnetic corrections for the samples were estimated from Pascal's constants.[6] Susceptibility measurements in solution were obtained by Evans method using a Bruker Avance 500 FT spectrometer operating at 500.1 MHz.[7] A diamagnetic correction for the sample,[6] and a correction for the variation of the density of the CD_3CN solvent with temperature,[8] were applied to these data. Thermodynamic parameters and spin-crossover midpoint temperatures were derived by fitting these data to eq 1 and 2, where nHS(T) is the high-spin fraction of the sample at temperature T:

$$\ln[(1- n\text{HS}(T))/n\text{HS}(T)] = \Delta H/RT - \Delta S/R \qquad (1)$$
$$\Delta S = \Delta H/T_{1/2} \qquad (2)$$

Equation 1 is a rearrangement of $\Delta G = -RT\ln K$, where K is the ratio of high-spin and low-spin molecules in the sample at temperature T; and, $\Delta G = \Delta H - T\Delta S$. Equation 2 reflects that, at $T_{1/2}$, the SCO is at equilibrium so $\Delta G = 0$ and $\Delta H = T_{1/2}\Delta S$.

Table S1. Experimental data for the organic ligand single crystal structures. All data were collected using synchrotron radiation.

	L^1C_{12}	L^2C_{12}	L^2C_{14}
formula	$C_{23}H_{29}N_5$	$C_{23}H_{33}N_5$	$C_{25}H_{37}N_5$
fw	375.51	379.54	407.60
crystal system	monoclinic	triclinic	triclinic
space group	$P2_1$	$P\bar{1}$	$P\bar{1}$
a / Å	5.3937(2)	5.3890(1)	5.3976(1)
b / Å	5.4359(2)	10.1738(1)	10.1852(1)
c / Å	35.4175(15)	19.2473(3)	20.8348(3)
α / deg	–	95.529(1)	87.345(1)
β / deg	90.977(3)	94.405(1)	84.116(1)
γ / deg	–	90.258(1)	89.840(1)
V / Å^3	1038.28(7)	1047.18(3)	1138.15(3)
Z	2	2	2
T / K	100(2)	100(2)	100(2)
D_{calcd} / g cm^{-3}	1.201	1.204	1.189
μ / mm^{-1}	0.069	0.069	0.068
reflections measured	10313	15685	18066
unique reflections	2284	8455	9489
R_{int}	0.094	0.068	0.109
$R_1 [I > 2\sigma(I)]$[a]	0.090	0.054	0.061
wR_2 [all data][b]	0.240	0.149	0.180
GOF	1.128	0.972	1.032
Flack parameter	2(7)[c]	–	–
CCDC	2064046	2064047	2064048

[a]$R = \Sigma\ [\,|F_o| - |F_c|\,] / \Sigma |F_o|$　　[b]$wR = [\Sigma w(F_o^2 - F_c^2)^2 / \Sigma wF_o$　　[c]The absolute structure for this light atom crystal could not be defined by the data.

Table S2. Experimental data for the single crystal structure of $[Fe(L^2C_{12})_2][BF_4]_2$, and unit cell data from more weakly diffracting crystals of isostructural $[Fe(L^2C_{16})_2][BF_4]_2$ and $[Fe(L^2C_{18})_2][BF_4]_2$. Data were collected using synchrotron radiation, unless otherwise stated.

	$[Fe(L^2C_{12})_2][BF_4]_2$	$[Fe(L^2C_{16})_2][BF_4]_2$[a]	$[Fe(L^2C_{18})_2][BF_4]_2$
formula	$C_{46}H_{66}B_2F_8FeN_{10}$	$C_{54}H_{82}B_2F_8FeN_{10}$	$C_{58}H_{90}B_2F_8FeN_{10}$
fw	988.56	1100.77	1156.87
crystal system	triclinic	triclinic	triclinic
space group	$P\bar{1}$	$P\bar{1}$	$P\bar{1}$
a / Å	10.8639(2)	10.9510(14)	10.9192(5)
b / Å	15.2602(3)	15.0831(18)	15.1344(5)
c / Å	30.1058(6)	34.713(4)	36.7856(17)
α / deg	97.198(2)	83.845(10)	84.117(4)
β / deg	97.749(2)	82.536(10)	85.034(4)
γ / deg	90.119(2)	89.868(10)	89.951(3)
V / Å^3	4905.63(16)	5652(1)	6024.1(3)
Z	4	4	4
T / K	100(2)	150(2)	100(2)
D_{calcd} / gcm^{-3}	1.338	1.294	1.276
μ / mm^{-1}	0.382	–	–
reflections measured	57066	–	–
unique reflections	23637	–	–
R_{int}	0.164	–	–
$R_1 [I > 2\sigma(I)]$[a]	0.076	–	–
wR_2 [all data][b]	0.216	–	–
GOF	0.880	–	–
CCDC	2064049	–	–

[a]Collected using Cu-K_α radiation. [b]$R = \Sigma [|F_o| - |F_c|] / \Sigma |F_o|$ [c]$wR = [\Sigma w(F_o^2 - F_c^2)^2 / \Sigma wF_o$

The unit cell angles are either >90° or all <90° for the different compounds, depending on which of these settings was selected by the merging software for each dataset. Despite that inconsistency, these are isostructural unit cells.

Preliminary structure solutions showed $[Fe(L^2C_{16})_2][BF_4]_2$ and $[Fe(L^2C_{18})_2][BF_4]_2$ are isomorphous with their C_{12} congener (Figures S25 and S26). However the crystals diffracted more weakly, such that anisotropic refinement of the full structures were not justified. The partial refinements were employed for the powder pattern simulations in Figure S30, but have not been deposited on the Cambridge Crystallographic Database.

Organic Ligands
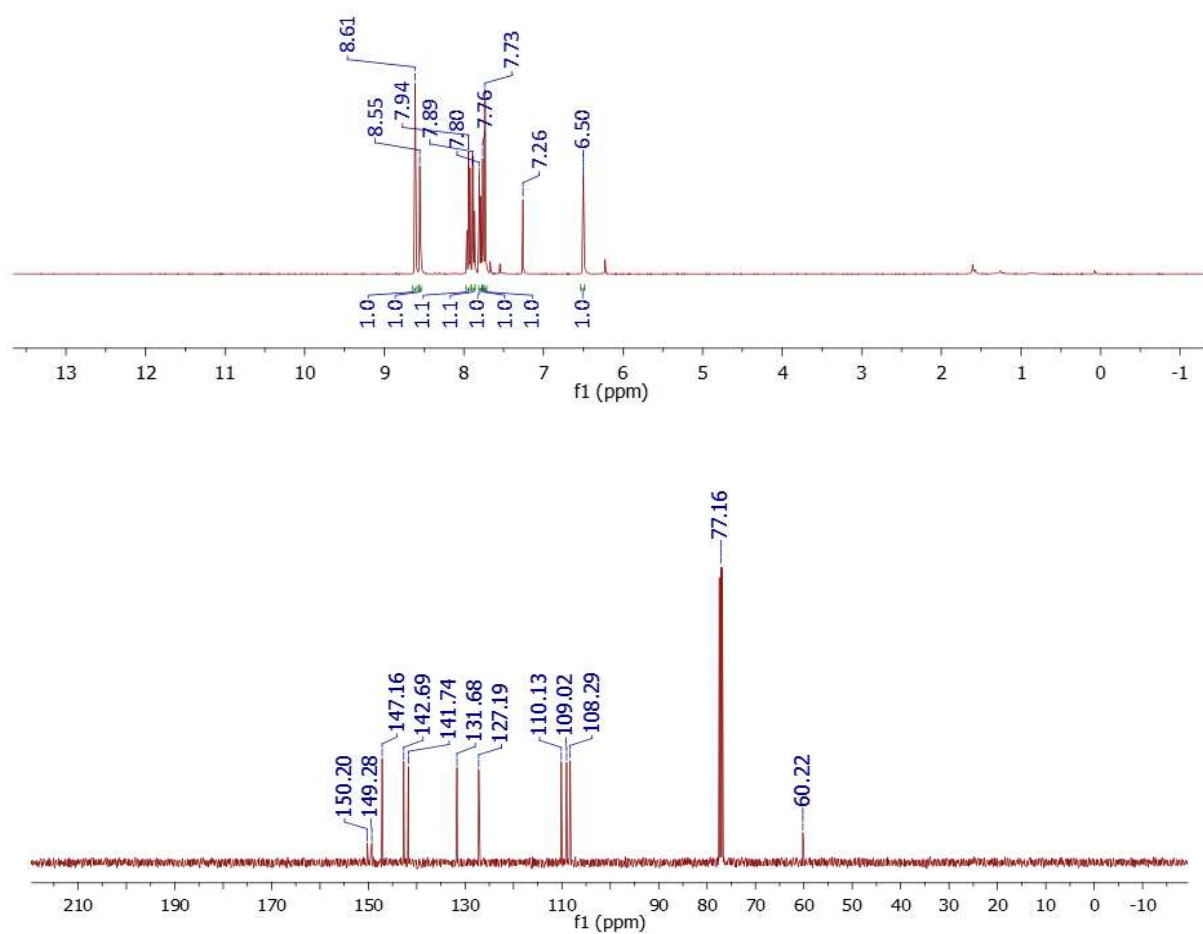
Figure S1 ^{1}H and ^{13}C NMR spectra of 2-(4-iodopyrazol-1-yl)-6-(pyrazol-1-yl)pyridine (CDCl$_3$).
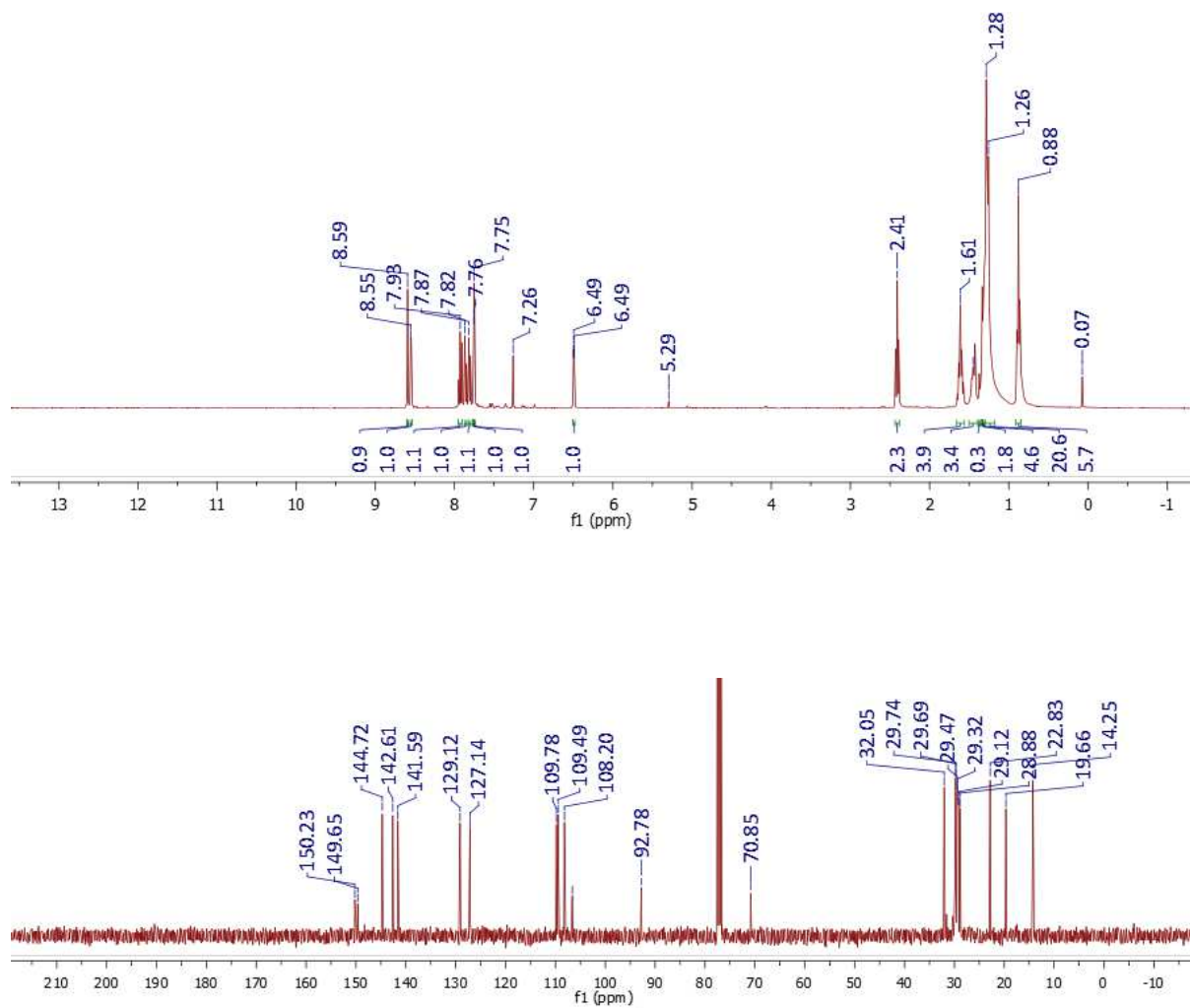
Figure S2 ^{1}H and ^{13}C NMR spectra of L^1C_{12} (CDCl$_3$).
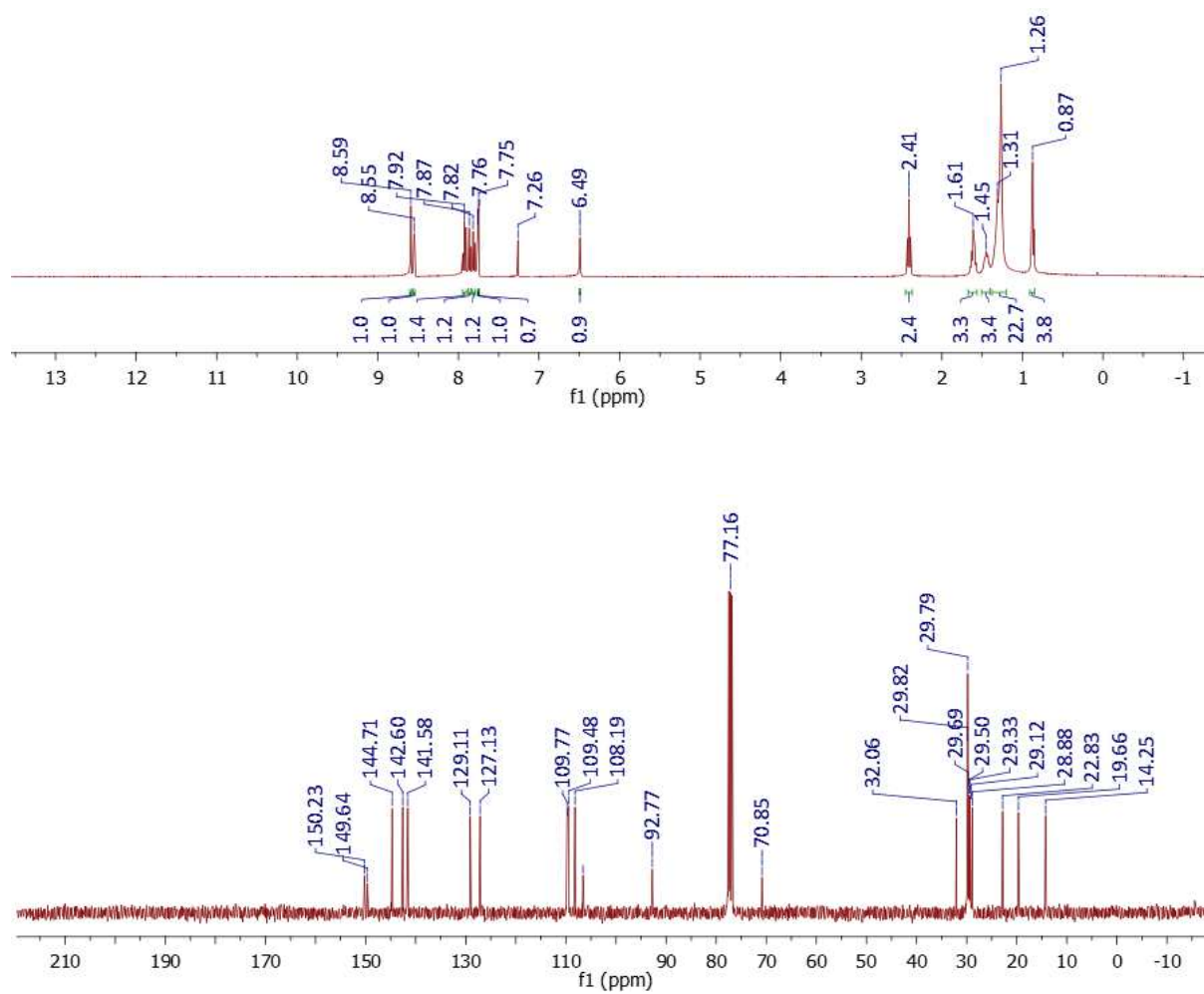
Figure S3 ^{1}H and ^{13}C NMR spectra of L^1C_{14} (CDCl$_3$).
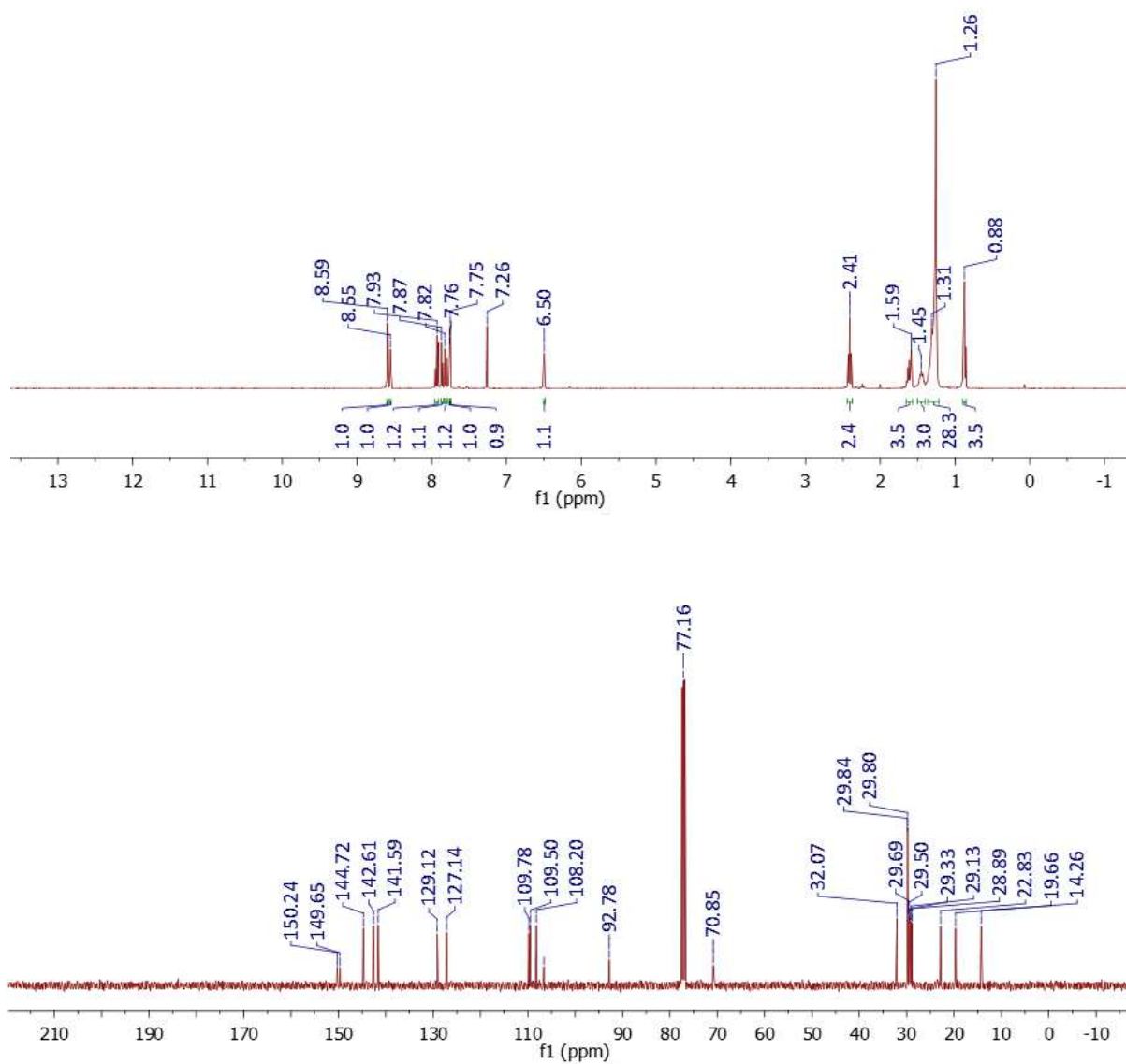
Figure S4 ^{1}H and ^{13}C NMR spectra of L^1C_{16} (CDCl$_3$).
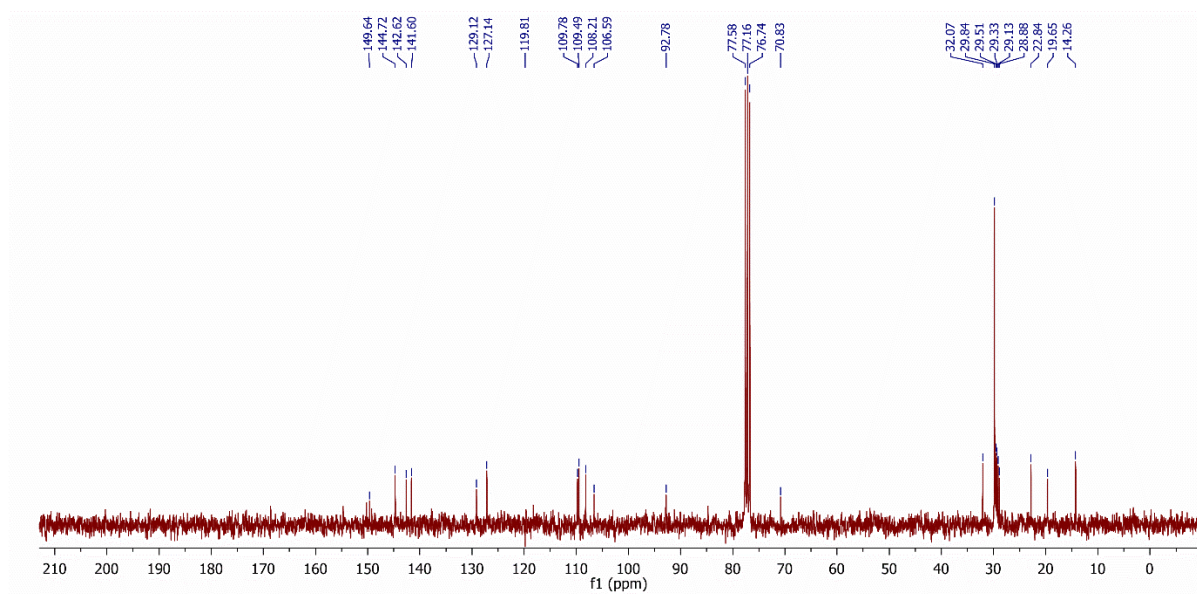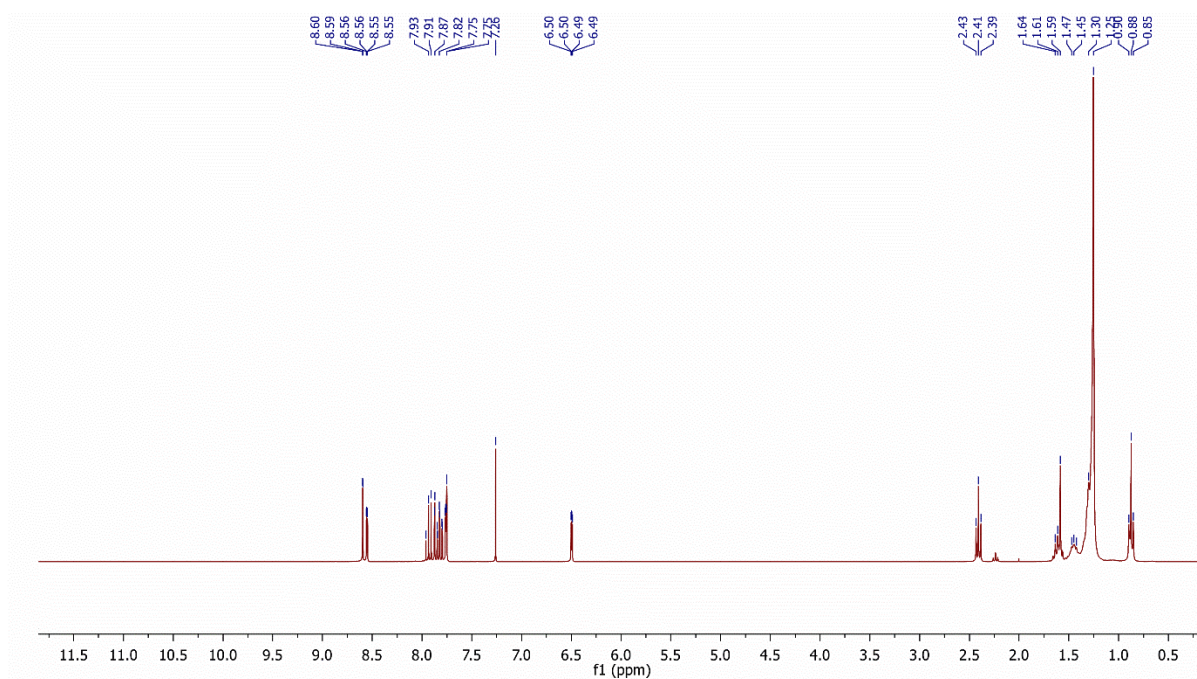
Figure S5 ^1H and ^{13}C NMR spectra of L^1C_{18} (CDCl$_3$).
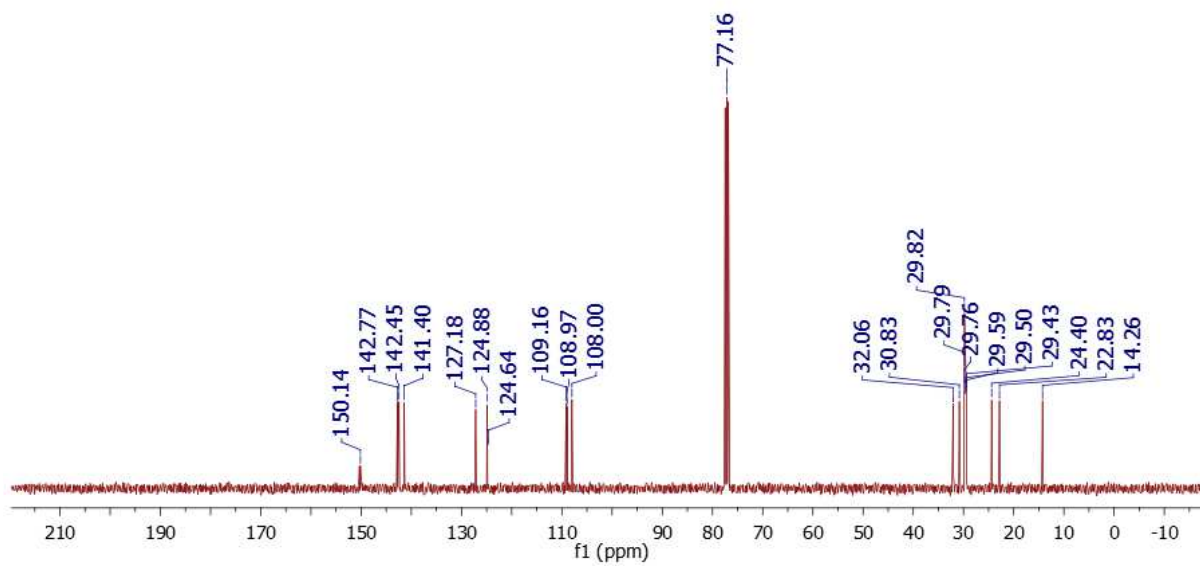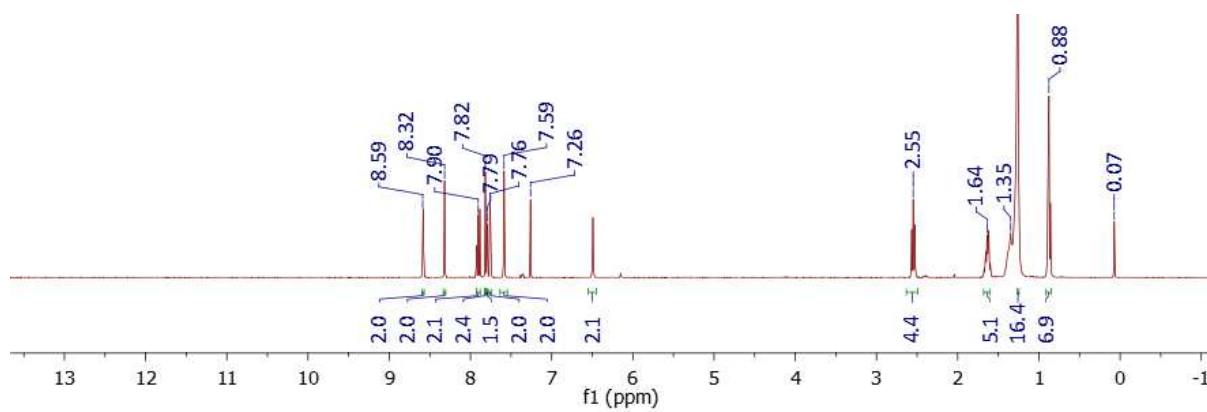
Figure S6 ^{1}H and ^{13}C NMR spectra of L^2C_{12} (CDCl$_3$).
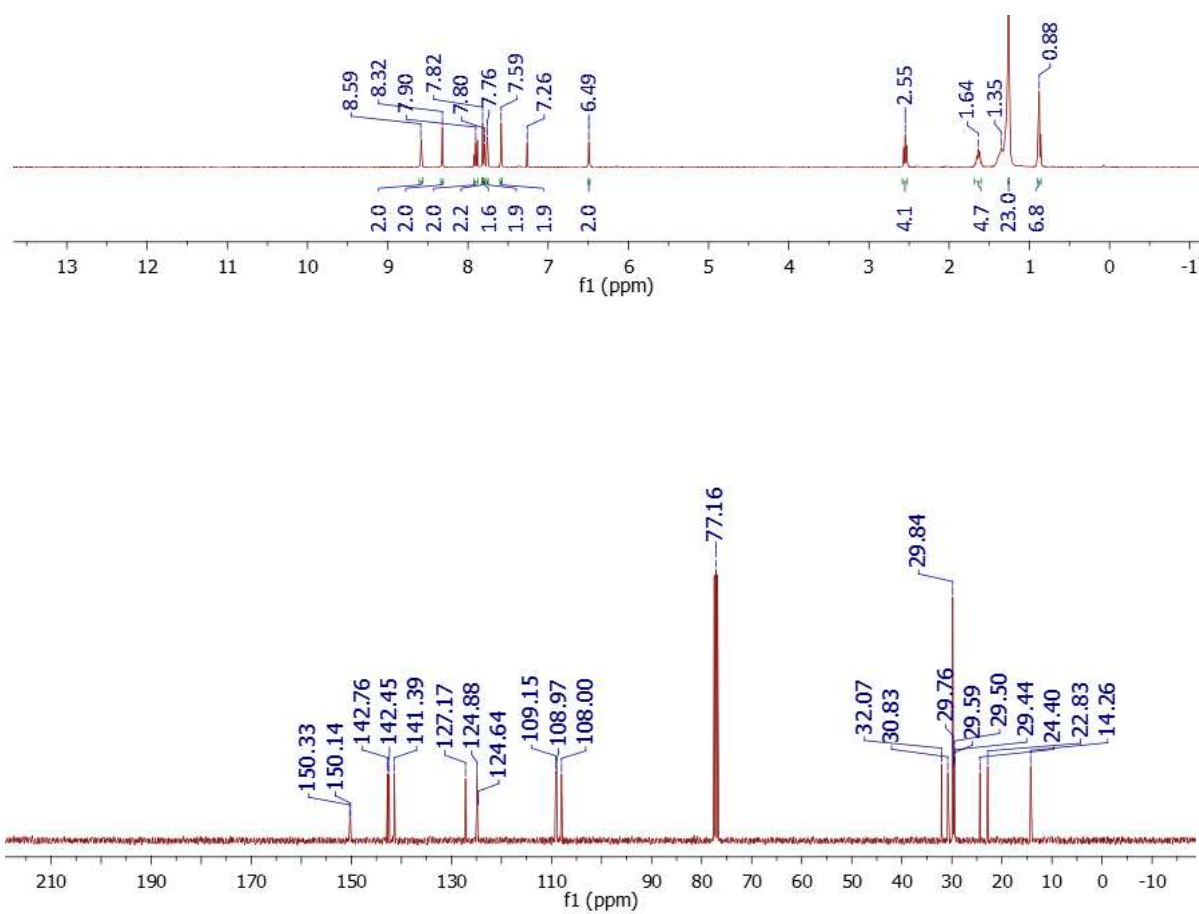
Figure S7 ^{1}H and ^{13}C NMR spectra of L^2C_{14} (CDCl$_3$).
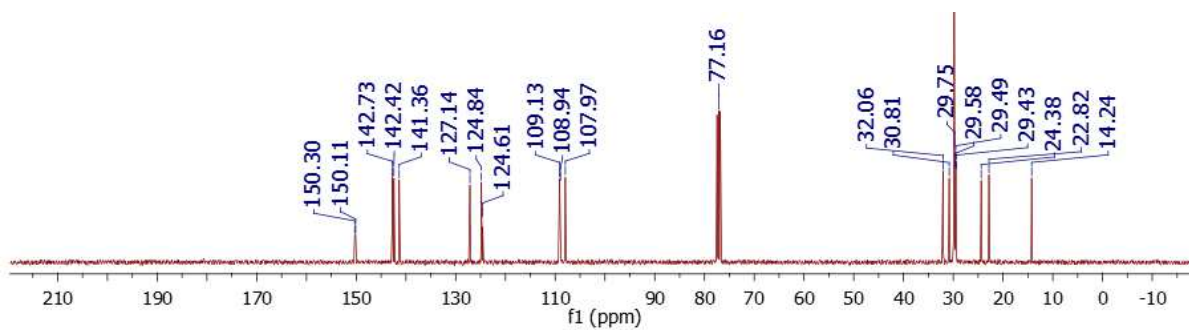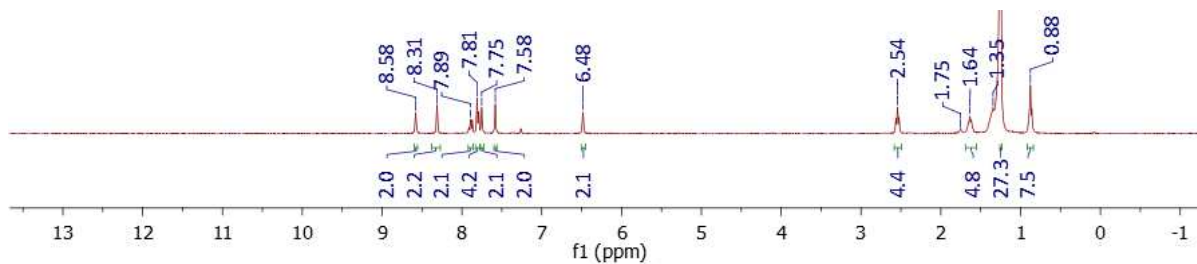
Figure S8 ^{1}H and ^{13}C NMR spectra of L^2C_{16} (CDCl$_3$).
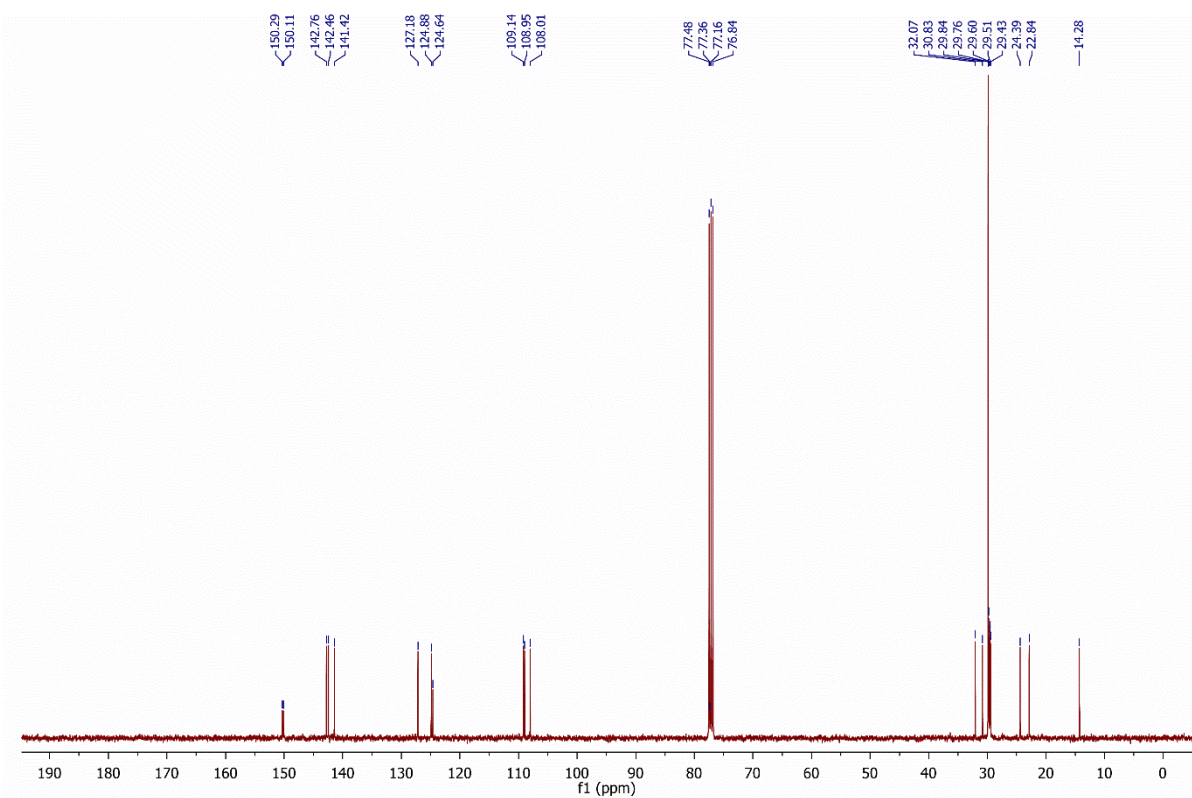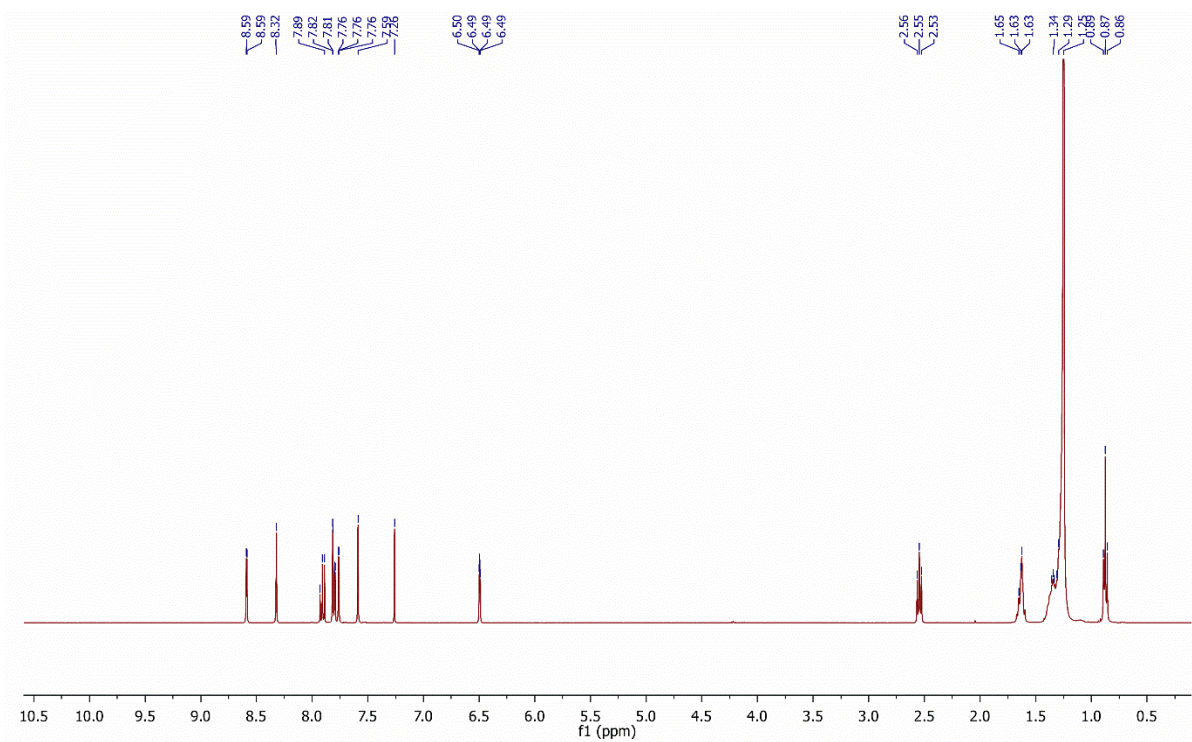
Figure S9 ^{1}H and ^{13}C NMR spectra of L^2C_{18} (CDCl$_3$).
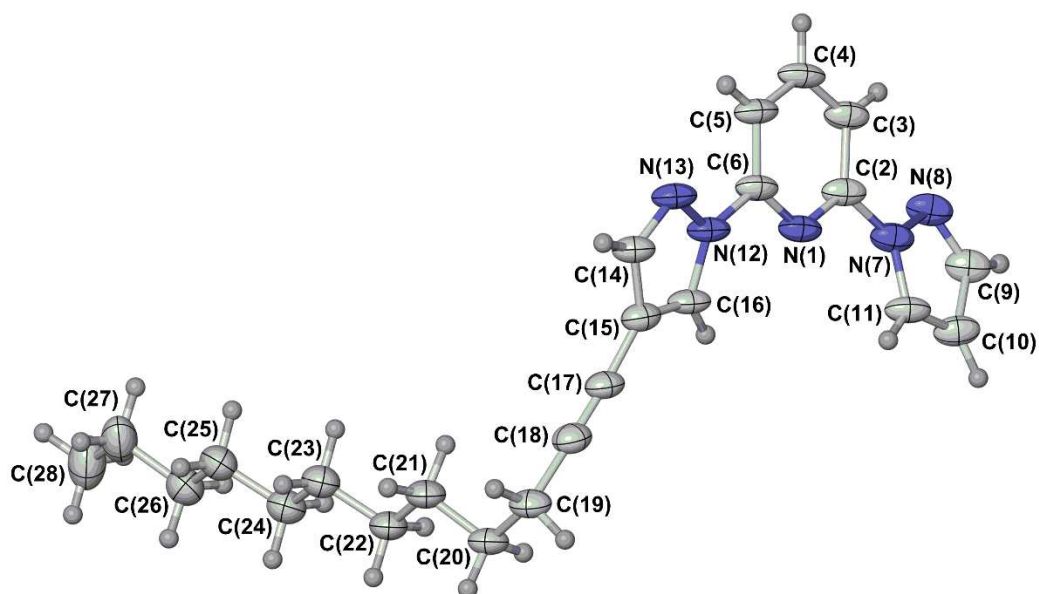
Figure S10 View of the molecule in the crystal structure of L^{1}C$_{12}$. Displacement ellipsoids are at the 50 % probability level except for H atoms which have arbitrary radii. Colour code: C, white; H, grey; N, blue.
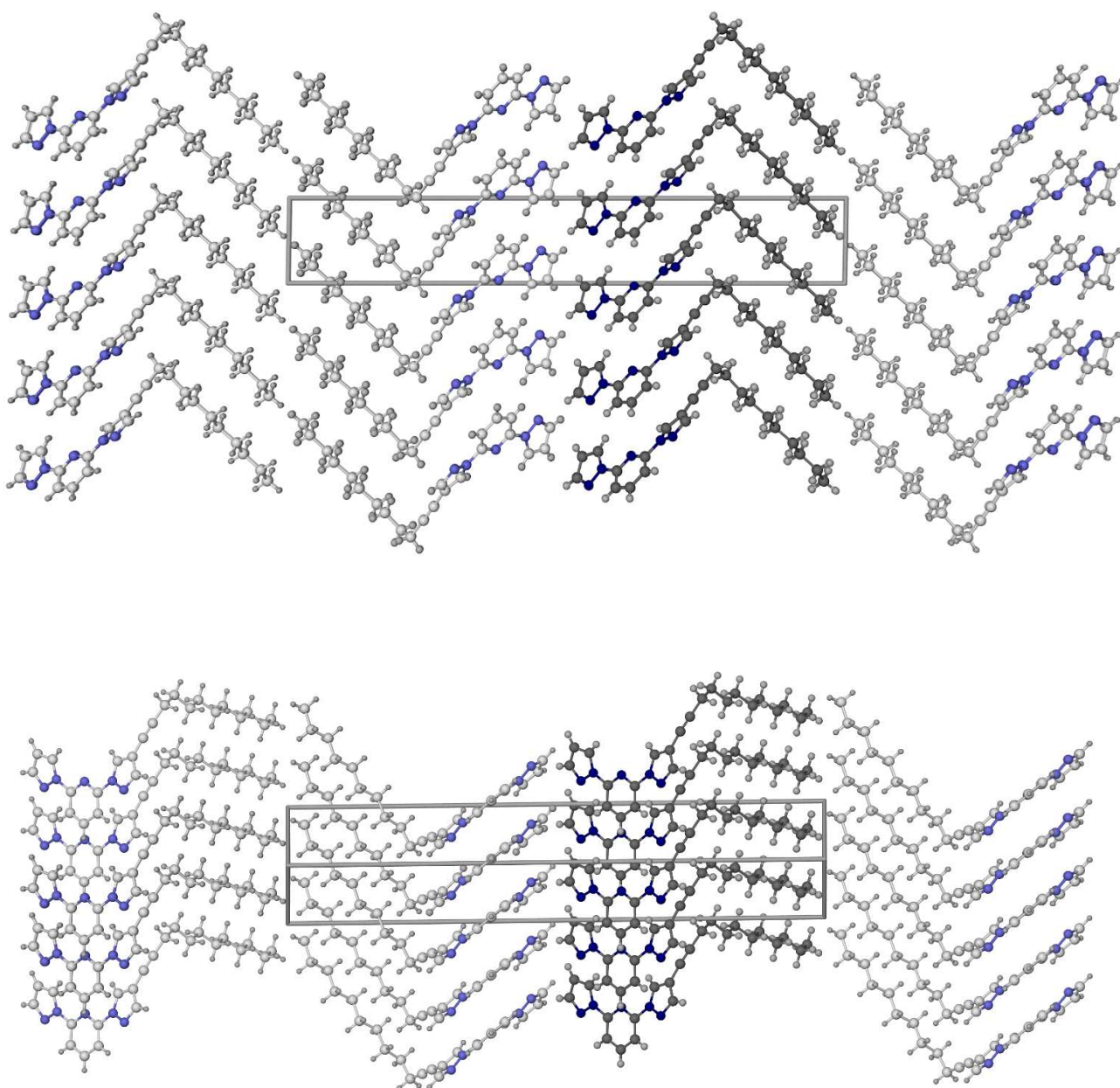
Figure S11 Views of the crystal packing of L^1C_{12}. Top: viewed parallel to the [010] crystallographic vector, with *c* horizontal. Bottom, viewed along the [010] crystal vector with the *c* axis horizontal. One layer of π-stacked molecules is highlighted with dark colouration in each view. Colour code: C, white or dark grey; H, pale grey; N, pale or dark blue.

The heterocyclic core of each molecule is oriented approximately within the (110) or ($\bar{1}$10) crystal planes. Each molecule exhibits significant π-π overlap with its nearest neighbours related by translation along both *x* and *y*, leading to layers of overlapping molecules in the (001) plane. The heterocyclic cores of adjacent molecules in each layer are coplanar by symmetry, and are separated and horizontally offset by 3.026(9) Å and 4.47 Å (symmetry code 1+*x*, *y*, *z*), and by 3.104(9) Å and 4.46 Å (symmetry code *x*, 1+*y*, *z*).

The layers are arranged pairwise in the lattice by the crystallographic 2_1 axis.
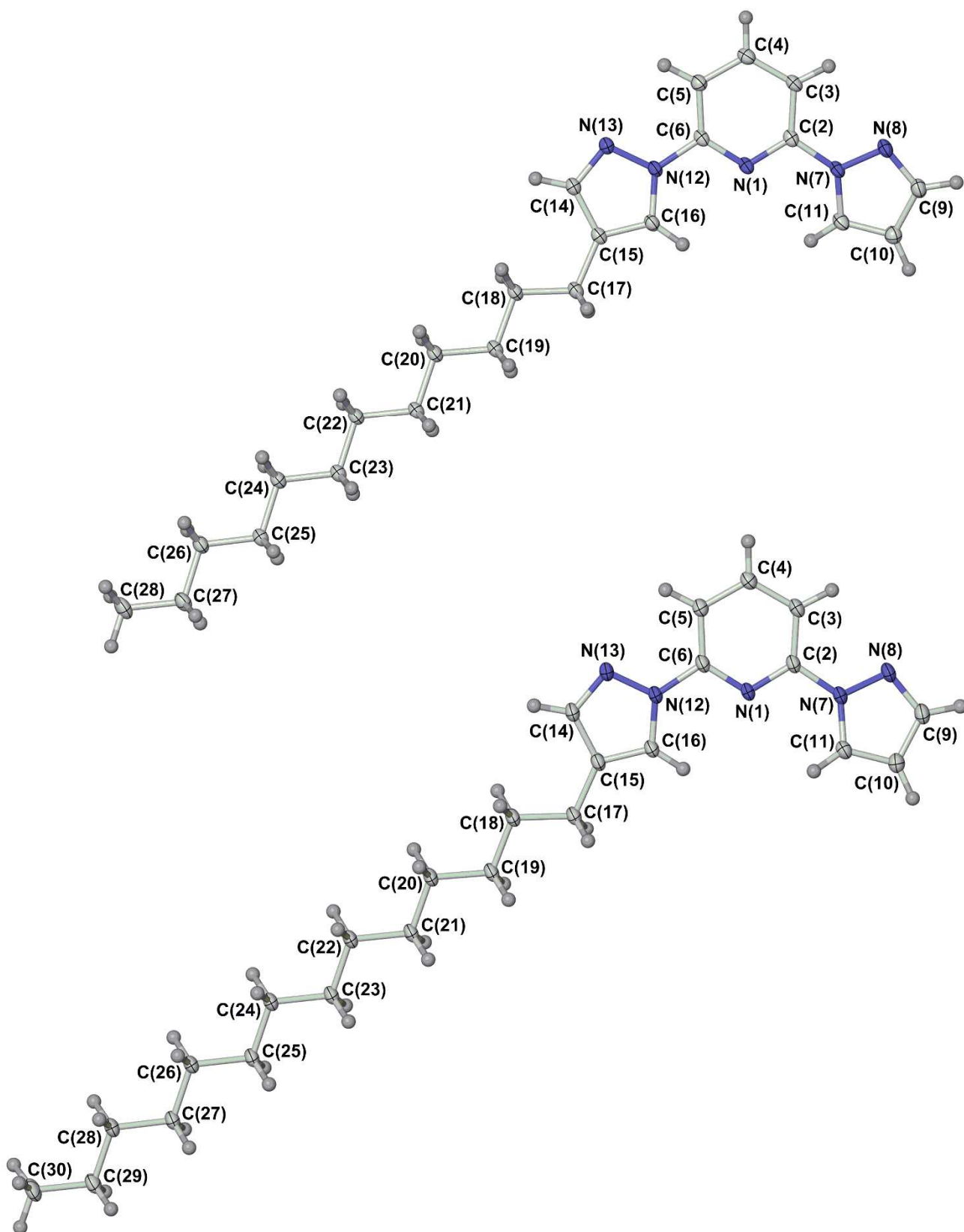
Figure S12 View of the molecules in the crystal structures of isomorphous L^2C_{12} (top) and L^2C_{14} (bottom). Displacement ellipsoids are at the 50 % probability level except for H atoms which have arbitrary radii. Colour code: C, white; H, grey; N, blue.
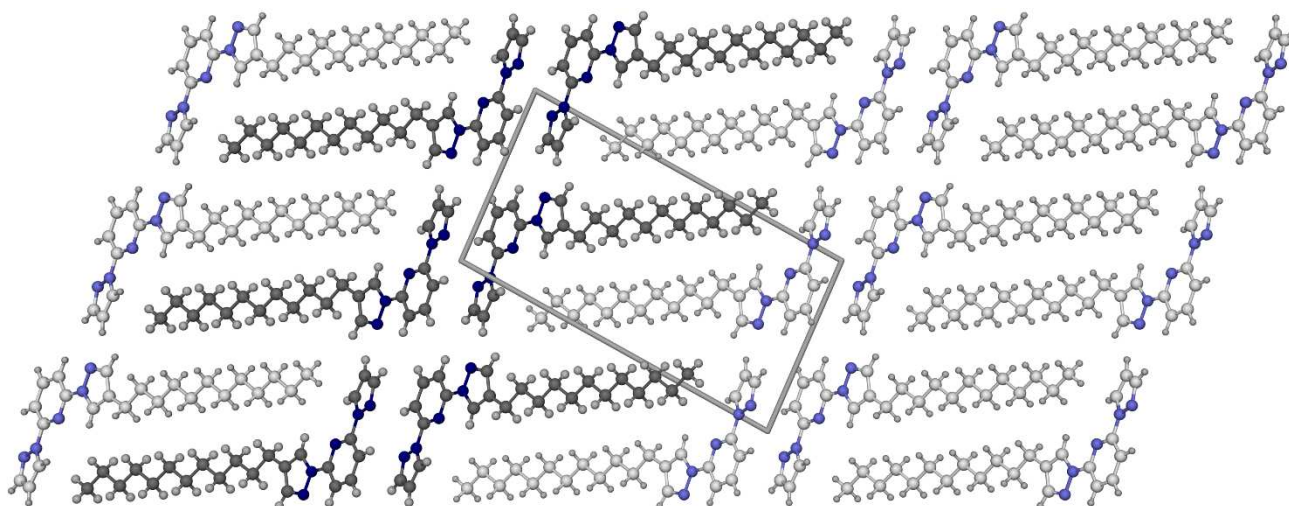
Figure S13 View of the crystal packing in L^2C_{12}, along the [100] crystal vector. One bilayer of π-stacked molecules is highlighted with dark colouration. Colour code: C, white or dark grey; H, pale grey; N, pale or dark blue.

The heterocyclic cores of the molecules form canted π-stacks by translation upon x, while the stacks in turn associate into bilayers through the crystallographic inversion centre. Nearest neighbour molecules in the bilayers are all coplanar by symmetry. The heterocyclic cores of adjacent molecules in the stacks are separated by 3.265(2) Å and offset horizontally by 4.29 Å (symmetry code $1+x$, y, z), while the corresponding dimensions for the second interaction forming the bilayers are 3.372(2) Å and 4.88 Å (symmetry code $3–x$, $–y$, $–z$).

The crystal packing in L^2C_{14} (which is is isomorphous with L^2C_{12}) is essentially the same as that shown here.
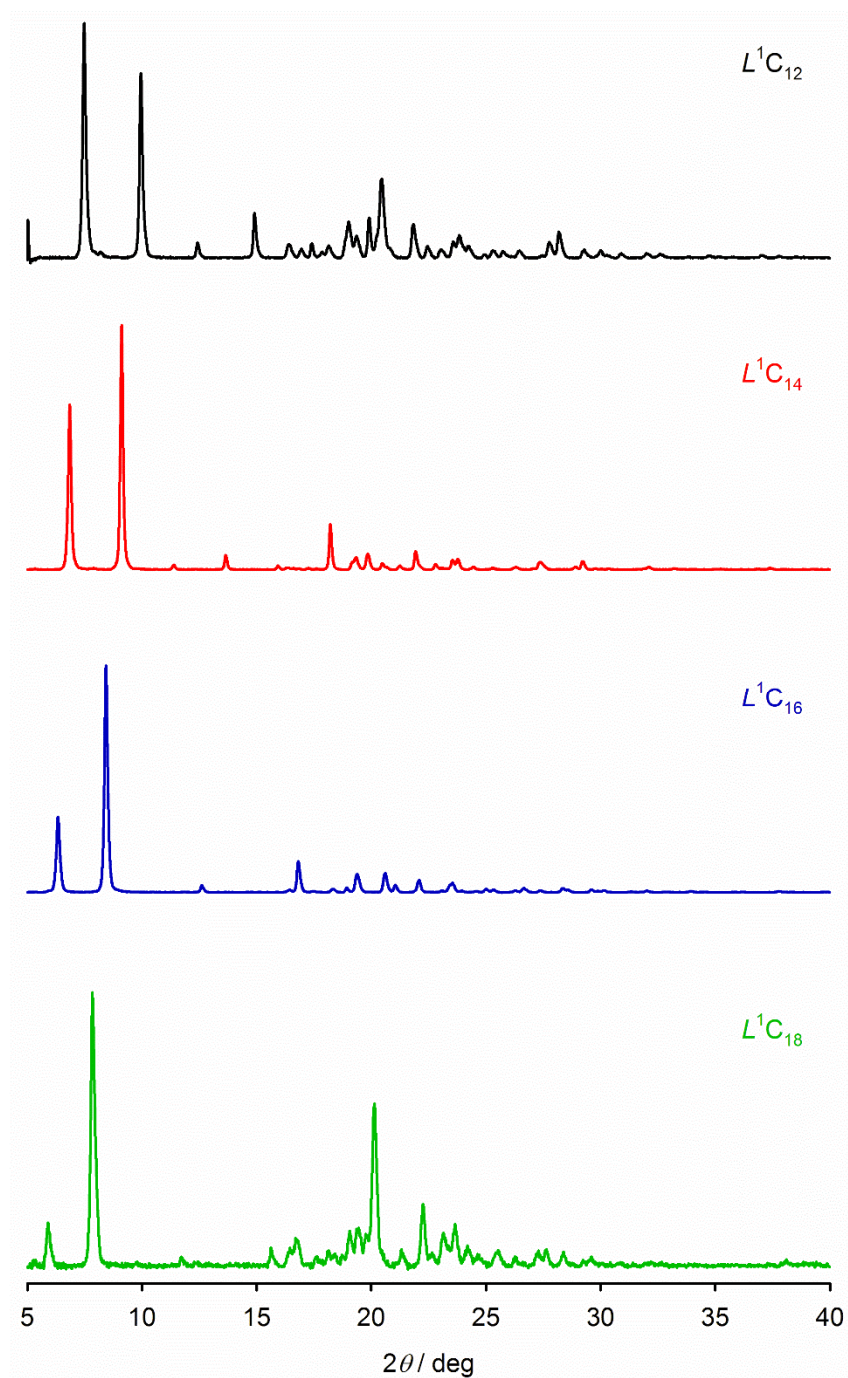
Figure S14 Room temperature X-ray powder diffraction data for the L^1C_m series of ligands.
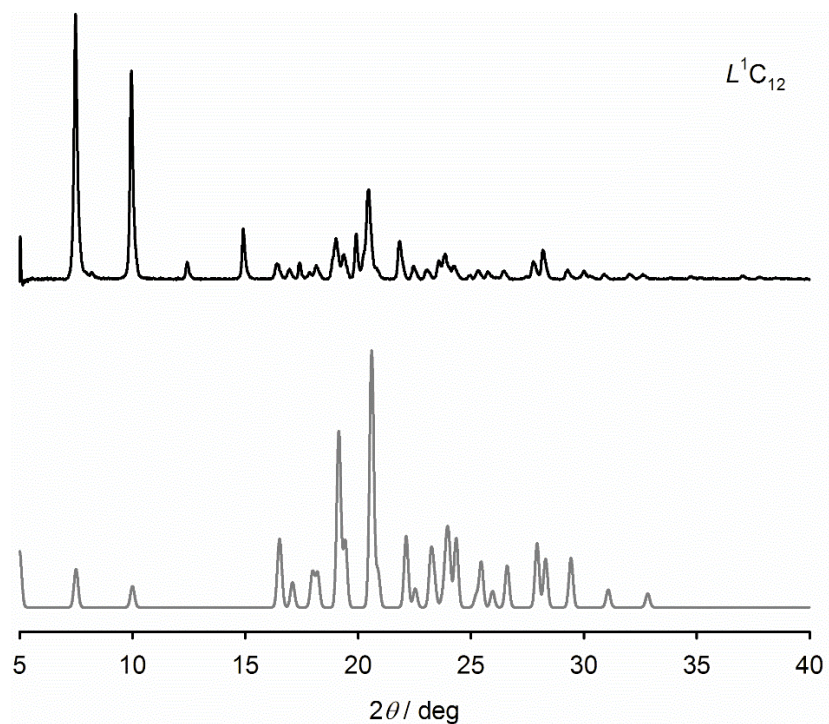
Figure S15 Measured (black or red) and simulated (grey) X-ray powder diffraction data for L^1C_{12}.

The single crystalline phase of this compound is the main component of the powder, although additional peaks near $2\theta = 12$ and $15°$ in the powder pattern imply a second phase may also be present. Discrepancies between observed and calculated peak intensities are common in measurements of this type, and can be ascribed to preferred orientation effects in the sample.
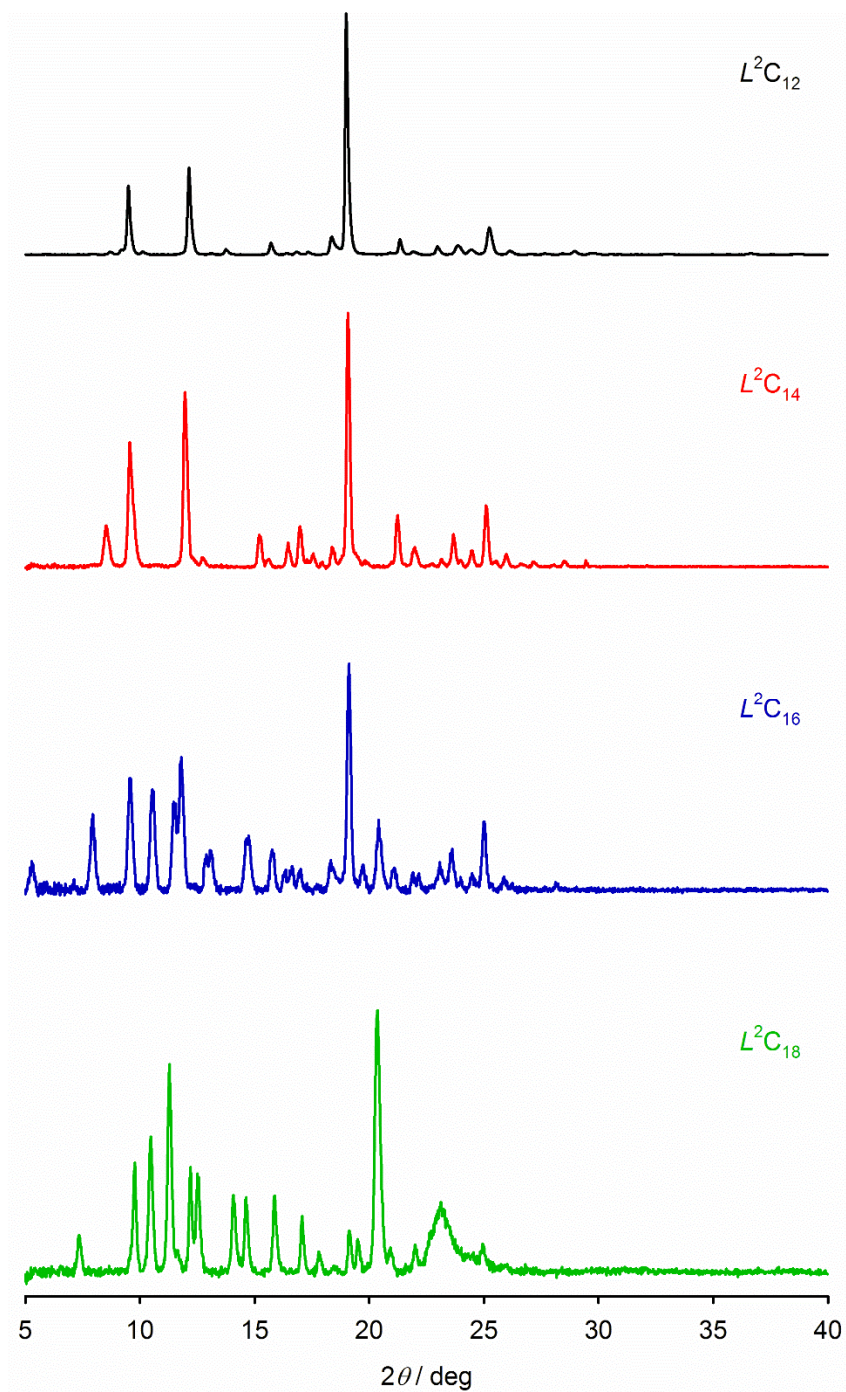
Figure S16 Room temperature X-ray powder diffraction data for the L^2C_m series of ligands.

These data imply L^2C_{12} and L^2C_{14} are isomorphous, as was found crystallographically, (Figure S13), but L^2C_{16} and L^2C_{18} adopt a different crystal phase. The broad feature near $2\theta = 22°$ in the data for L^2C_{18}, which was analytically pure, implies it may also contain some amorphous material.
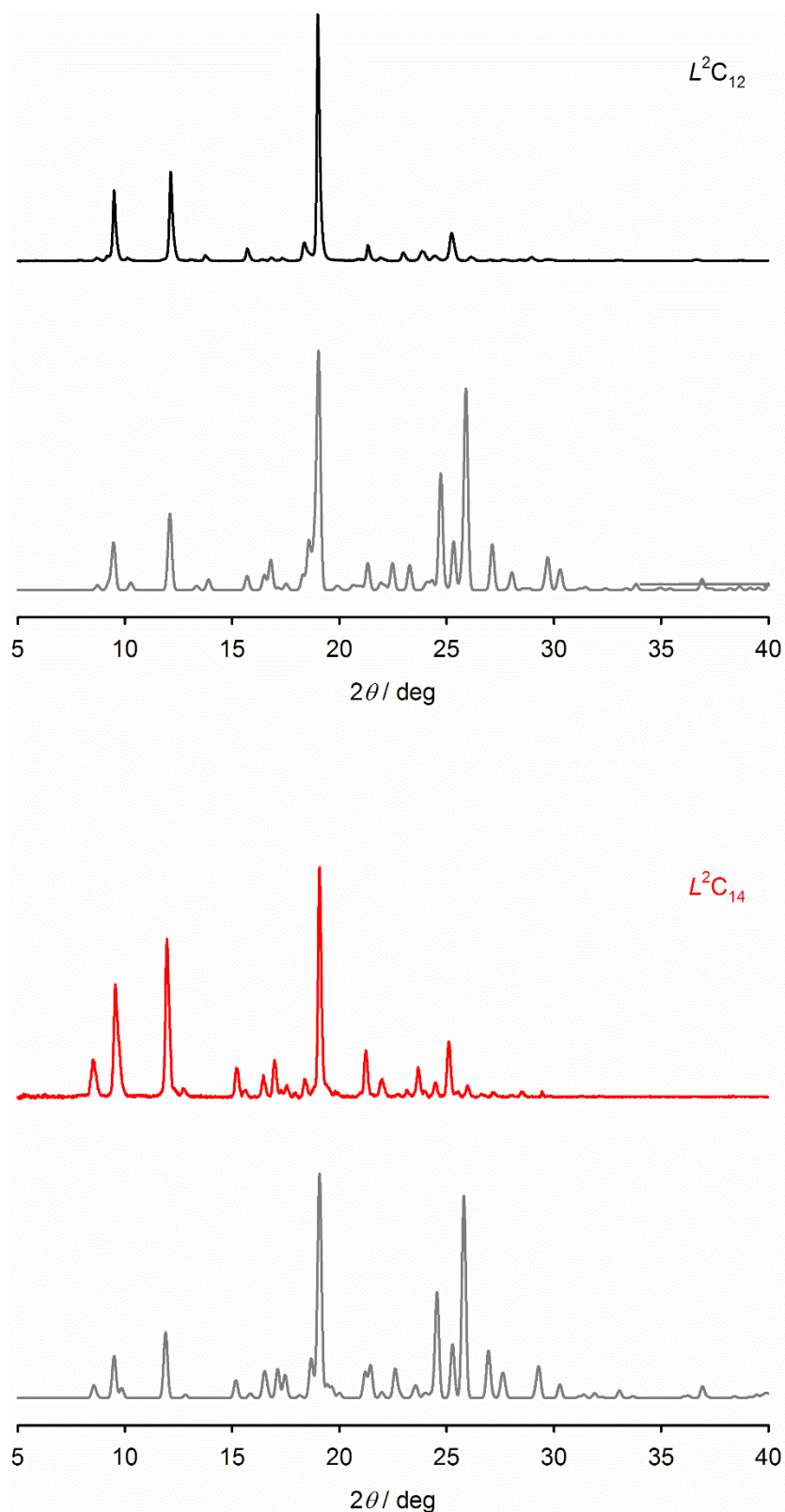
Figure S17 Measured (black or red) and simulated (grey) X-ray powder diffraction data for isostructural L^2C_{12} and L^2C_{14}.

Agreement between observed and calculated 2θ values is good for both compounds. Discrepancies between observed and calculated peak intensities are common in measurements of this type, and can be ascribed to preferred orientation effects in the sample.
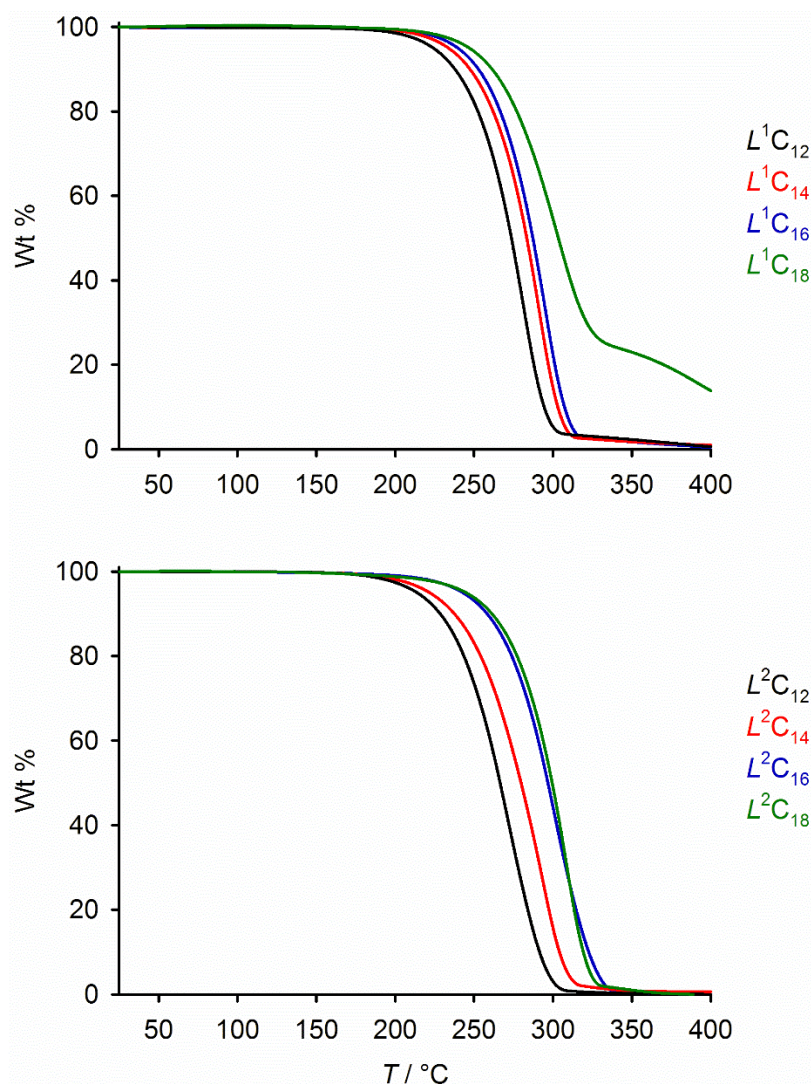
Figure S18 Thermogravimetric analysis (TGA) data for the L^1C_m (top) and L^2C_m (bottom) ligand series.

None of the compounds undergoes significant decomposition until at least 100 °C above their melting points, which are 59-77 °C for L^1C_m and 67-84 °C for L^2C_m.
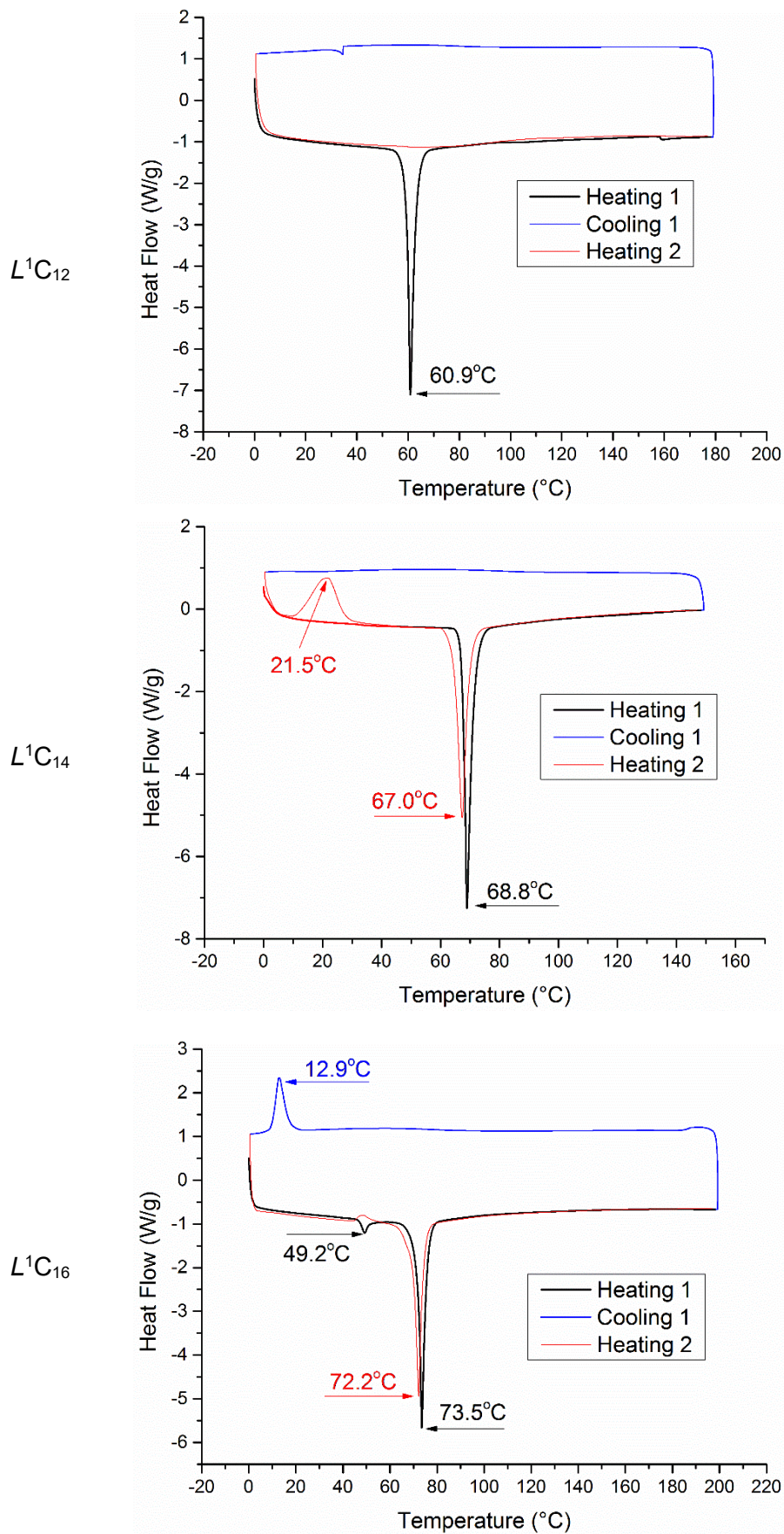
Figure S19 Differential Scanning Calorimetry (DSC) data for the organic ligands in this work (scan rate 10 K min^{-1}).

L^1C_{18}

L^2C_{12}

L^2C_{14}

Figure S19 (continued)

L^2C_{16}

L^2C_{18}
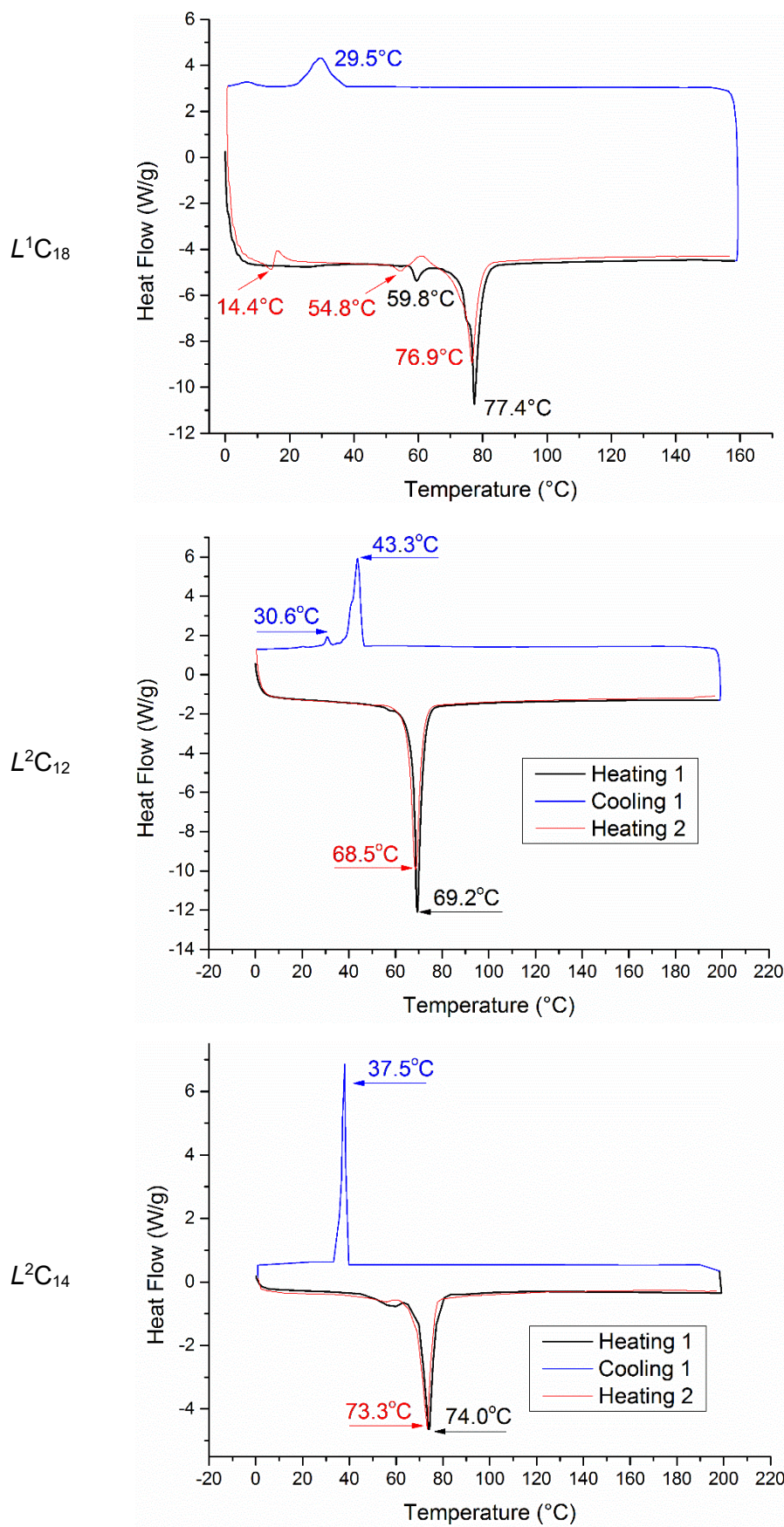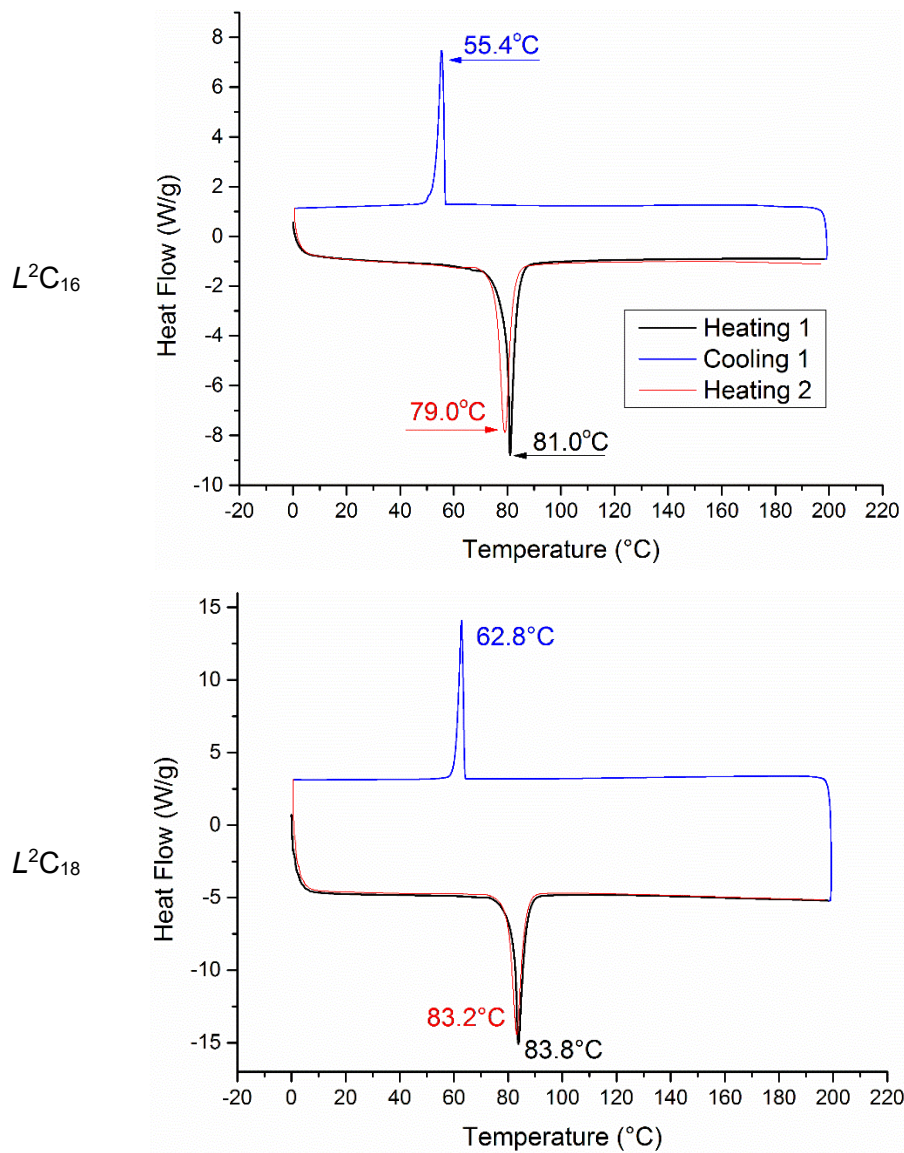
Figure S19 (continued)

Iron Complexes

[Fe(*L*¹C₁₂)₂][BF₄]₂ (CDCl₃)
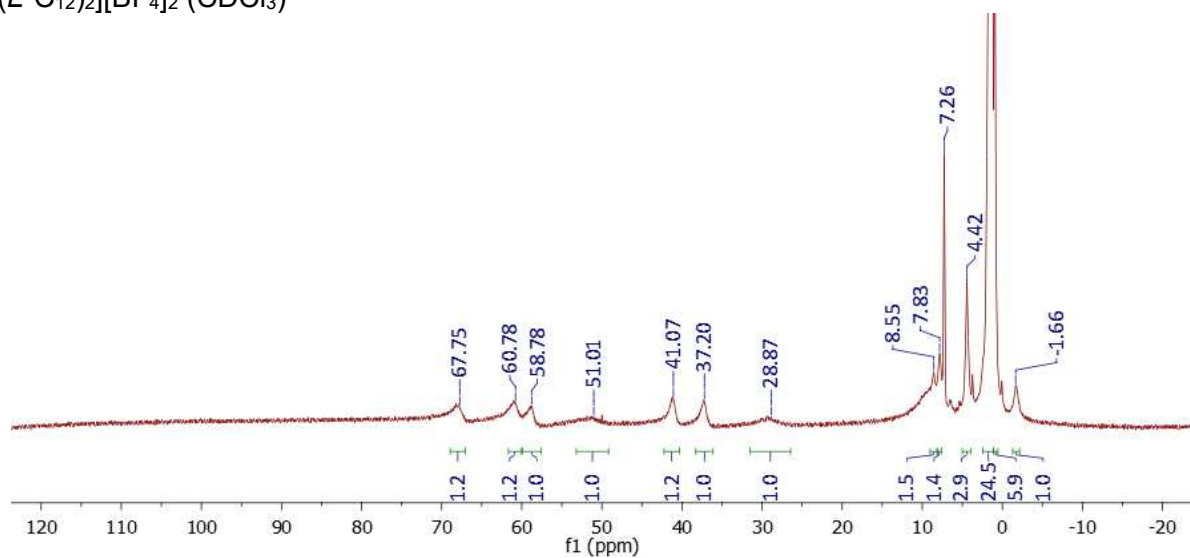
[Fe(*L*¹C₁₄)₂][BF₄]₂ (CDCl₃)
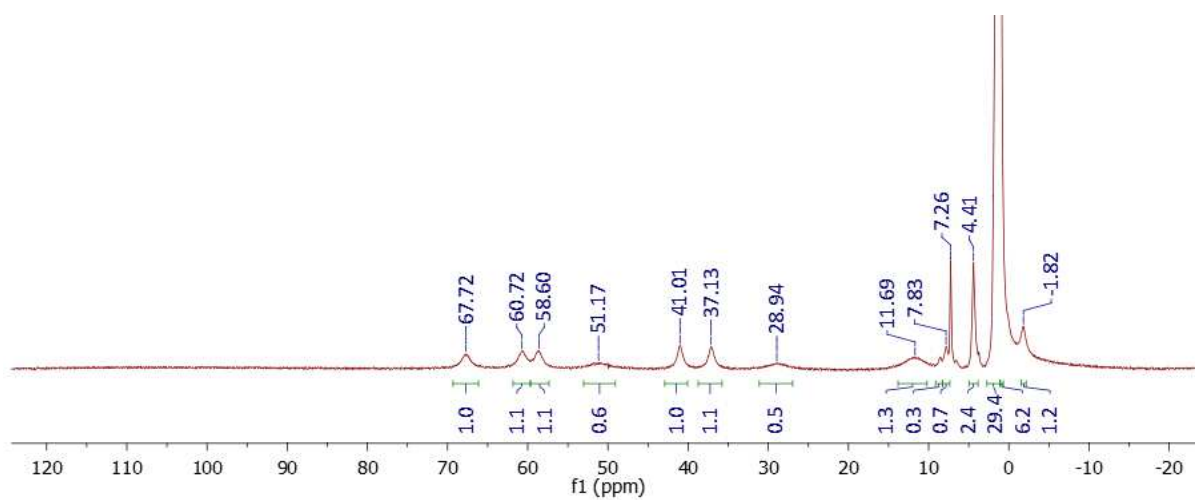
[Fe(*L*¹C₁₆)₂][BF₄]₂ (CDCl₃)
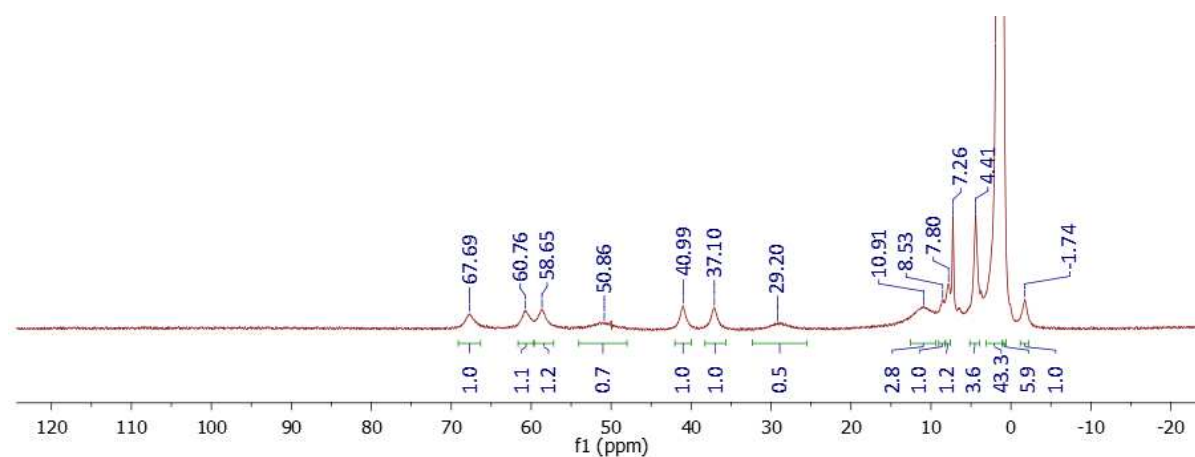
Figure S20 Paramagnetic ¹H NMR spectra of the complexes in this work.

[Fe(*L*²C₁₂)₂][BF₄]₂ (CD₃CN)
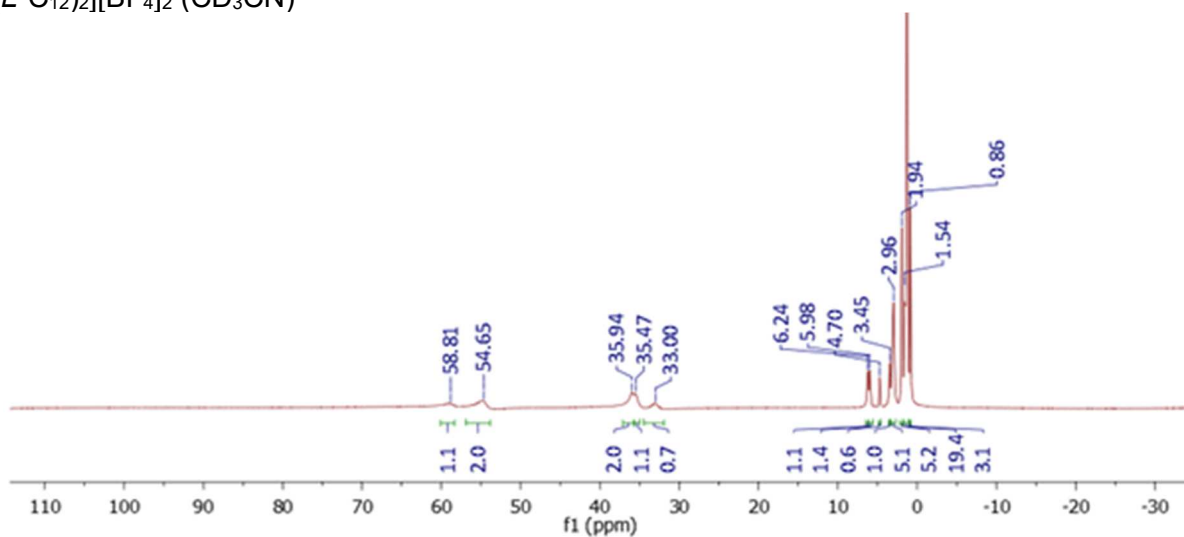
[Fe(*L*²C₁₄)₂][BF₄]₂ (CD₃CN)
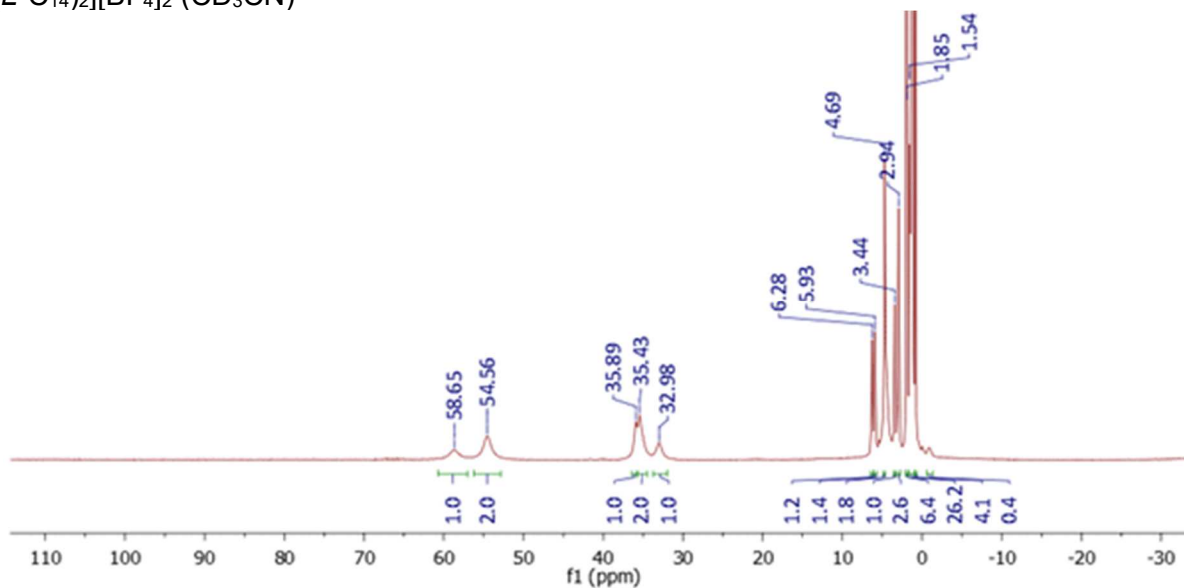
[Fe(*L*²C₁₆)₂][BF₄]₂ (CD₃CN)
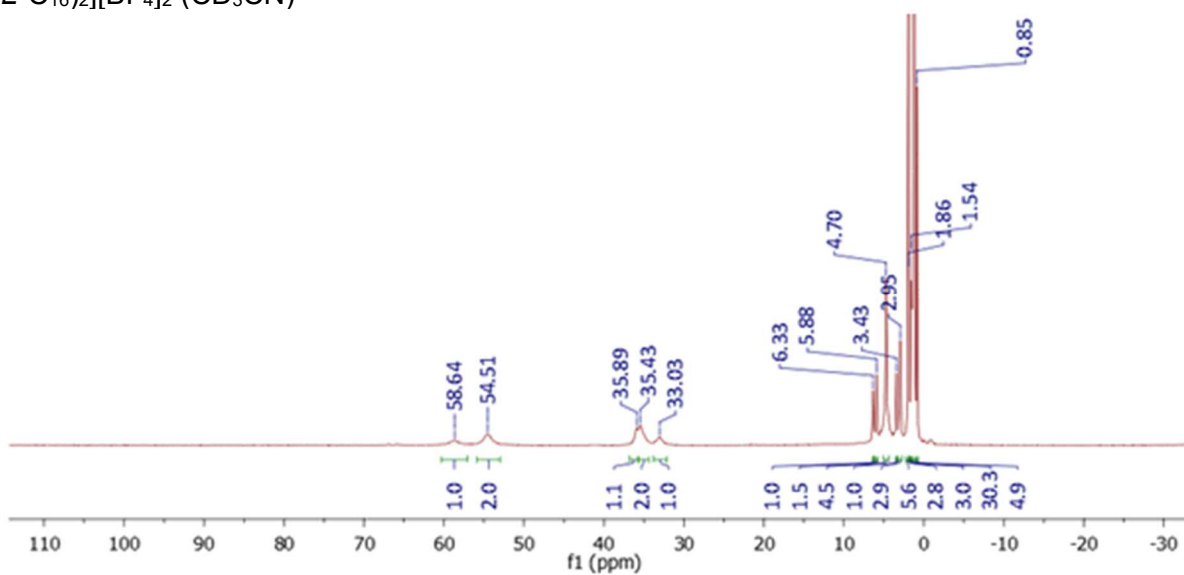
Figure S20 continued.
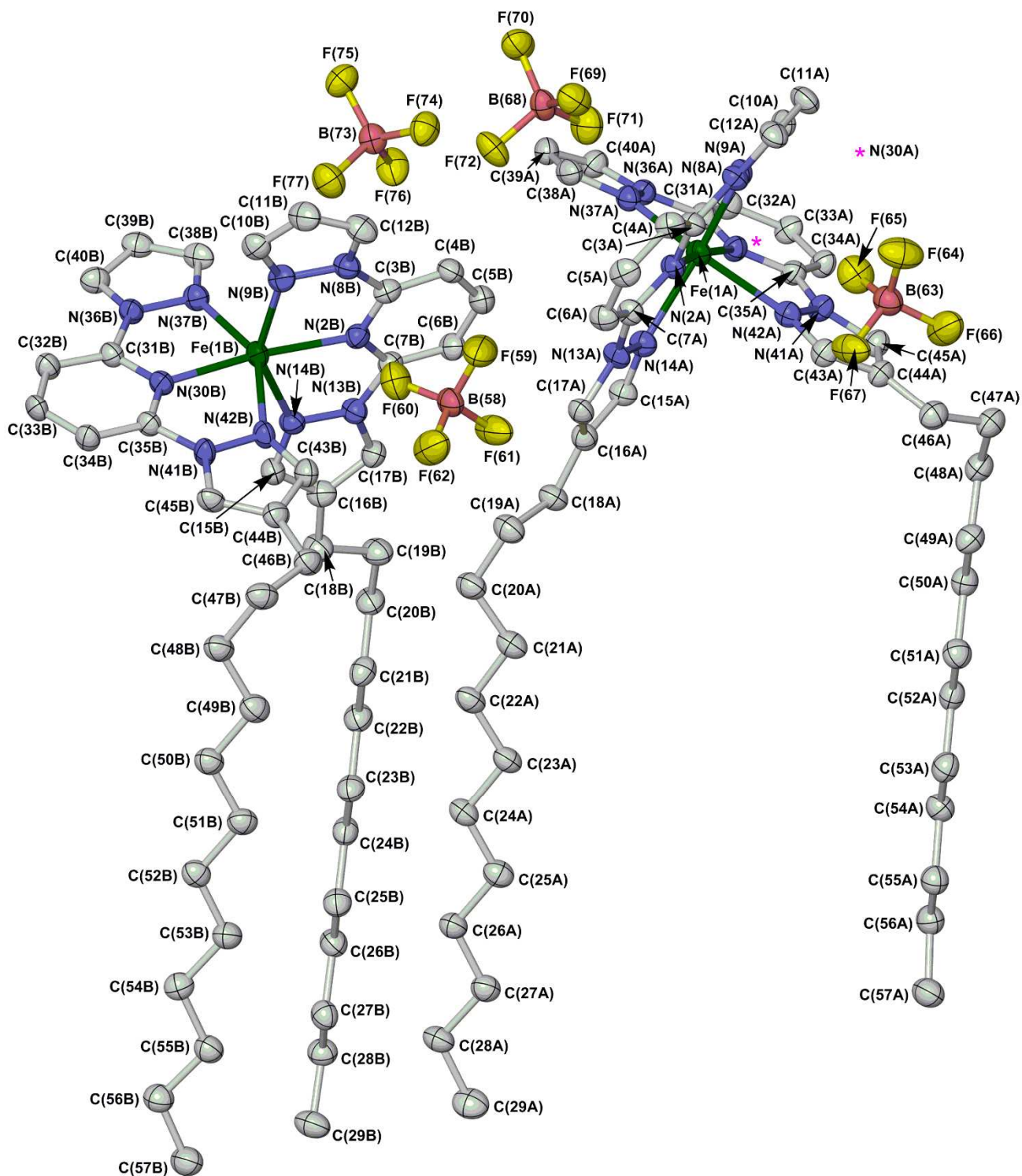
Figure S21 The asymmetric unit of [Fe(L^2C$_{12}$)$_2$][BF$_4$]$_2$, showing the full atom numbering scheme. Atomic displacement ellipsoids are at the 50 % probability level, and C-bound H atoms have been omitted for clarity. Colour code: C, white; B, pink; F, yellow; Fe, green; N, blue.

Table S3 Selected bond lengths and angles (Å, °) for [Fe(L^2C_{12})$_2$][BF$_4$]$_2$. See Figure S21 for the atom numbering scheme.

	Molecule A	Molecule B
Fe(1)–N(2)	2.117(3)	2.114(3)
Fe(1)–N(9)	2.180(3)	2.173(4)
Fe(1)–N(14)	2.199(3)	2.203(3)
Fe(1)–N(30)	2.115(3)	2.115(3)
Fe(1)–N(37)	2.170(3)	2.164(3)
Fe(1)–N(42)	2.236(3)	2.214(3)
N(2)–Fe(1)–N(9)	73.69(12)	73.81(13)
N(2)–Fe(1)–N(14)	73.32(12)	73.53(12)
N(2)–Fe(1)–N(30)	171.81(13)	171.81(13)
N(2)–Fe(1)–N(37)	114.17(12)	114.00(12)
N(2)–Fe(1)–N(42)	98.62(12)	98.52(12)
N(9)–Fe(1)–N(14)	146.98(12)	147.28(13)
N(9)–Fe(1)–N(30)	107.00(12)	106.49(13)
N(9)–Fe(1)–N(37)	97.65(12)	97.86(13)
N(9)–Fe(1)–N(42)	96.40(12)	95.97(13)
N(14)–Fe(1)–N(30)	105.46(12)	105.54(13)
N(14)–Fe(1)–N(37)	96.91(13)	97.09(12)
N(14)–Fe(1)–N(42)	87.21(12)	86.87(12)
N(30)–Fe(1)–N(37)	73.96(12)	74.17(12)
N(30)–Fe(1)–N(42)	73.19(12)	73.29(12)
N(37)–Fe(1)–N(42)	146.79(12)	147.07(12)
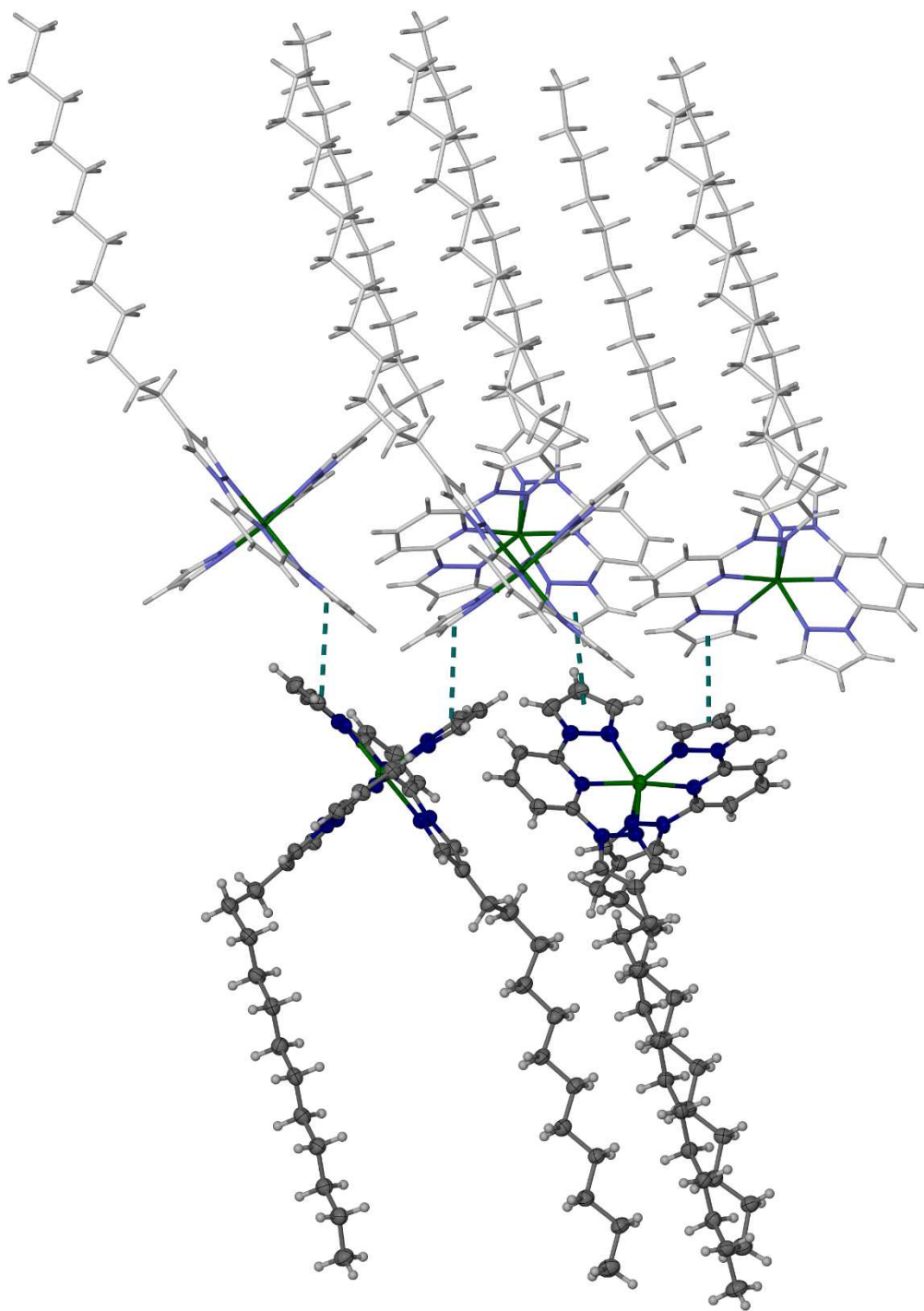
Figure S22 Nearest neighbour $\pi...\pi$ interactions between the cations in [Fe(L^2C$_{12}$)$_2$][BF$_4$]$_2$. The cations in the asymmetric unit are shown in dark colouration, while symmetry equivalent molecules are de-emphasised. The BF$_4^-$ ions are omitted for clarity.

Colour code C, white or dark grey; H, pale grey; Fe, green; N, pale or dark blue.

Each $\pi...\pi$ contact is generated by a crystallographic inversion centre. Hence, each A cation (on the left) interacts with two other A cations, and the B cation (right) interacts with two B-type nearest neighbours. Interacting pyrazolyl groups are coplanar by symmetry, and all four unique pairs have an interplanar spacing of 3.19(6) Å and are offset horizontally by 2.22-2.35 Å.
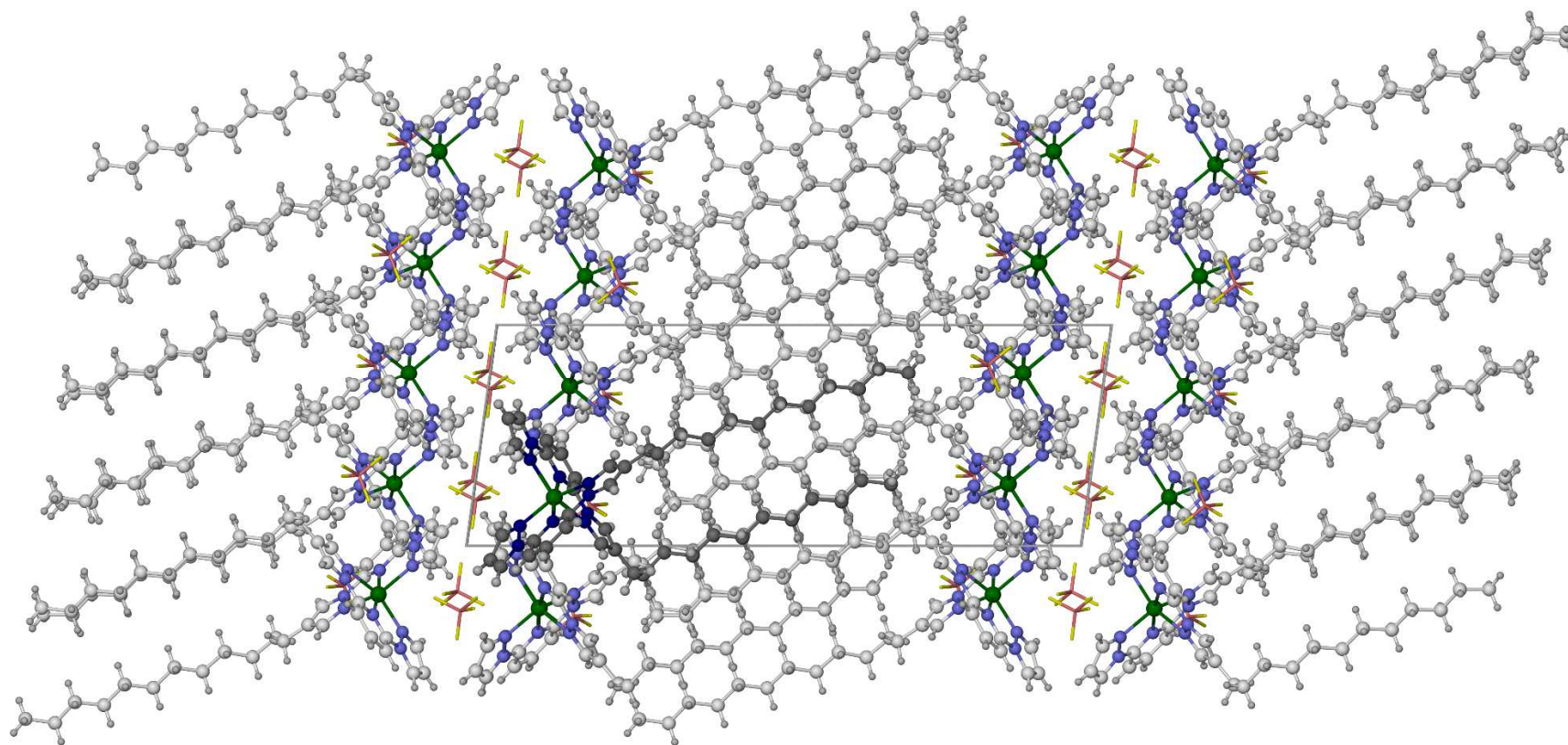
Figure S23 Packing diagram of $[Fe(L^2C_{12})_2][BF_4]_2$. The view is parallel to the [010] crystallographic vector, with *a* vertical. One cation is highlighted with dark colouration and the anions are de-emphasised, for clarity.

Colour code C, white or dark grey; H, pale grey; B, pink; F, yellow; Fe, green; N, pale or dark blue.

An alternative view of this packing is in Figure 1 of the main article.
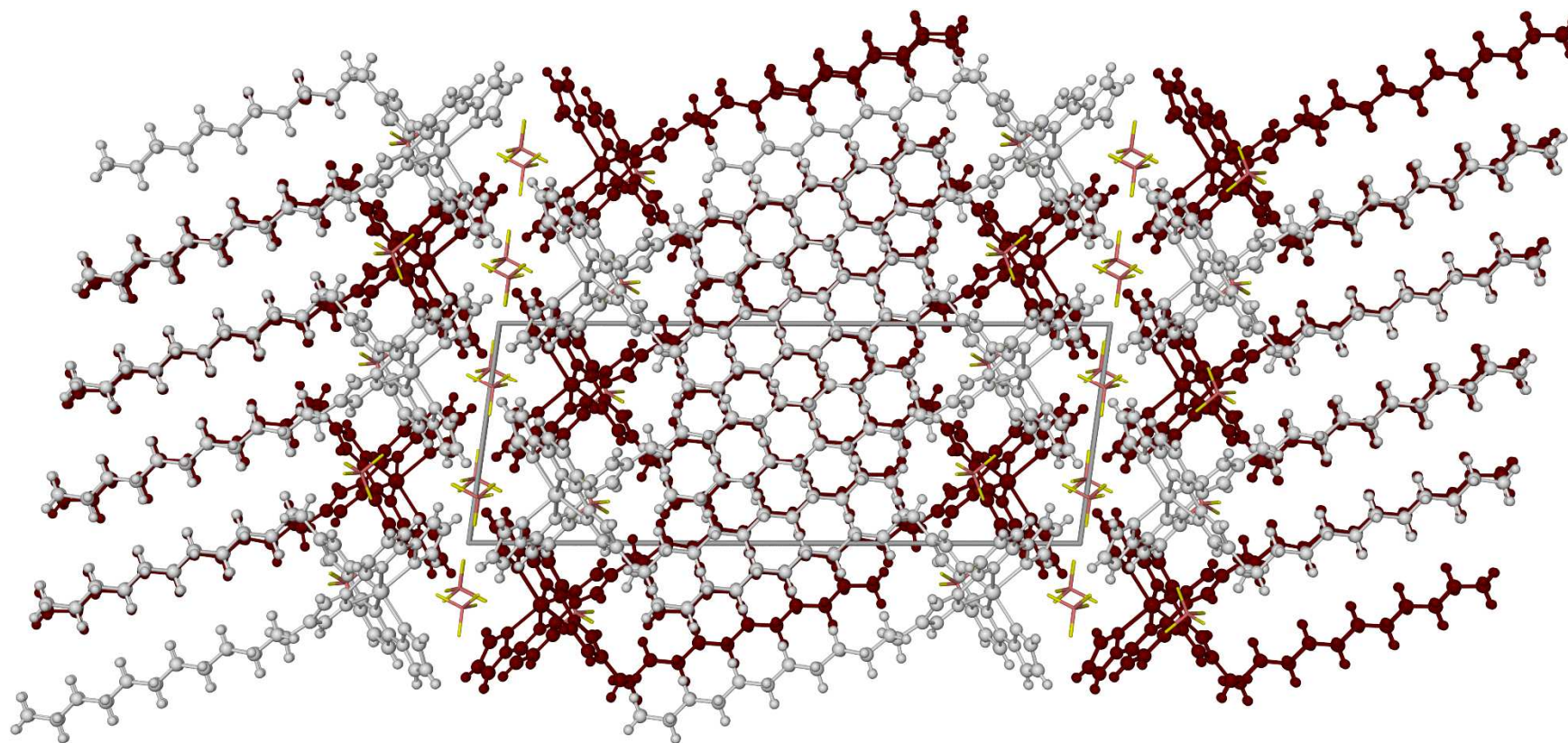
Figure S24 Packing diagram of [Fe(L^2C_{12})$_2$][BF$_4$]$_2$, showing the arrangement of the A (white) and B (maroon) cation environments in the lattice. The view is the same as in Figure S23.

The A and B cations are segregated into chains by the $\pi...\pi$ interactions in Figure S22, running parallel to the crystallographic a axis (which is vertical in the Figure).
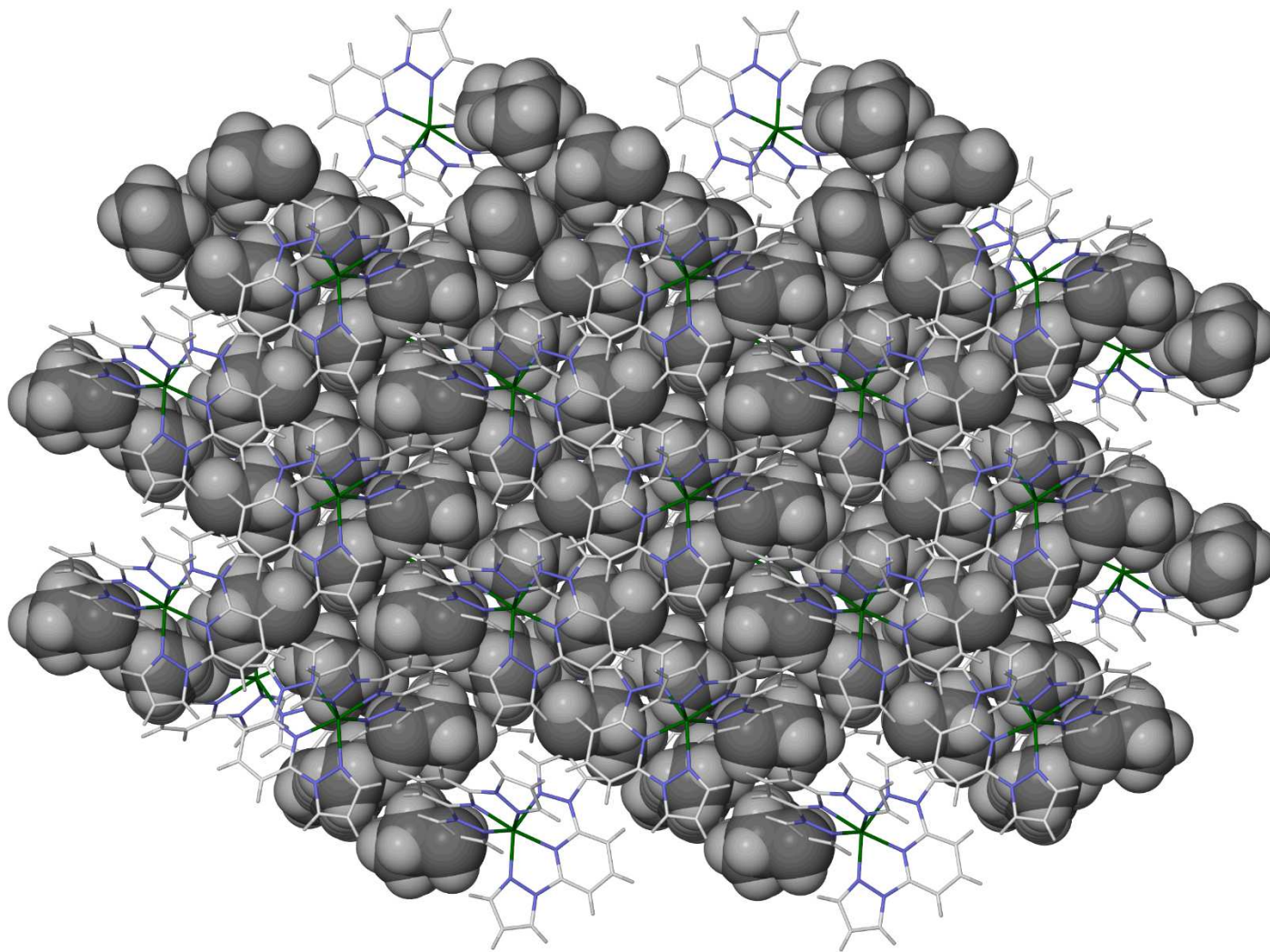
Figure S25 Space-filling packing diagram of the dodecyl chains within a lipid bilayer of $[Fe(L^2C_{12})_2][BF_4]_2$. Atoms from the $[Fe(bpp)_2]^{2+}$ core of the cations are de-emphasised, and the BF_4^- ions are omitted for clarity.

Colour code C{dodecyl}, dark grey; C{$[Fe(bpp)_2]^{2+}$ core}, white; H, pale grey; Fe, green; N, blue.

The dodecyl chains pack in an approximately hexagonal array. The closest C...C distances between nearest-neighbour chains lie between 4.0-4.4 Å, showing they are mostly in Van der Waals contact.
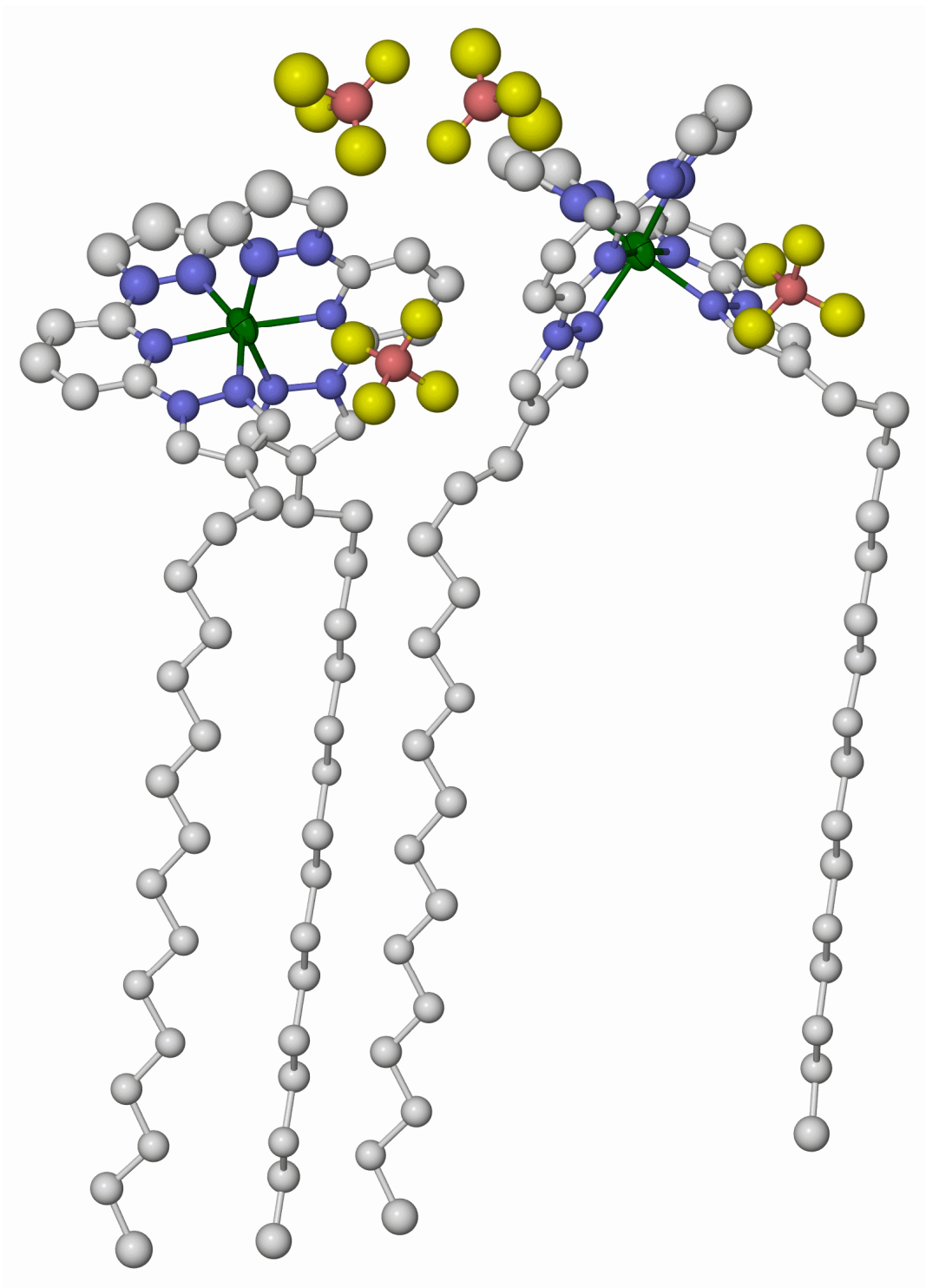
Figure S26 The asymmetric unit of [Fe(L^2C$_{16}$)$_2$][BF$_4$]$_2$, from the preliminary structure solution of that compound (Table S2). Atomic displacement ellipsoids are at the 50 % probability level, and C-bound H atoms have been omitted for clarity. Colour code: C, white; B, pink; F, yellow; Fe, green; N, blue.

Only 25 % of the data from this dataset were observed with $I > 2\sigma(I)$, which was insufficient for an anisotropic refinement. However, the compound is isomorphous with [Fe(L^2C$_{12}$)$_2$][BF$_4$]$_2$ (Figure S21), and the main features of these structures and [Fe(L^2C$_{18}$)$_2$][BF$_4$]$_2$ (Figure S27) are all clearly the same.

This structure has not been deposited with the Cambridge Crystallographic Database.
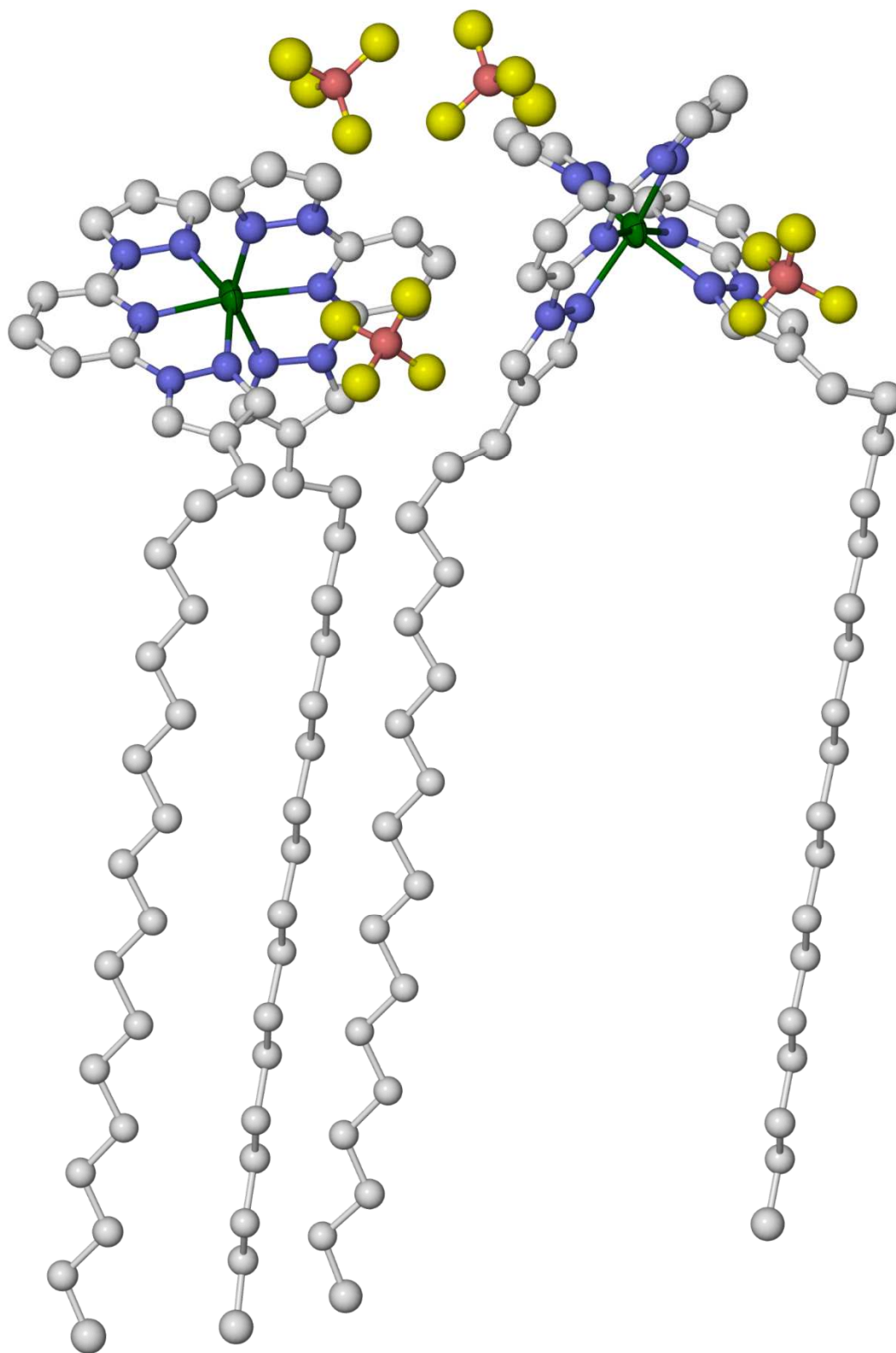
Figure S27 The asymmetric unit of [Fe(L^2C$_{18}$)$_2$][BF$_4$]$_2$, from the preliminary structure solution of that compound. Atomic displacement ellipsoids are at the 50 % probability level, and C-bound H atoms have been omitted for clarity. Colour code: C, white; B, pink; F, yellow; Fe, green; N, blue.

Only 32 % of the data from this dataset were observed with $I > 2\sigma(I)$, which was insufficient for an anisotropic refinement. Other comments as for Figure S26.

This structure has not been deposited with the Cambridge Crystallographic Database.
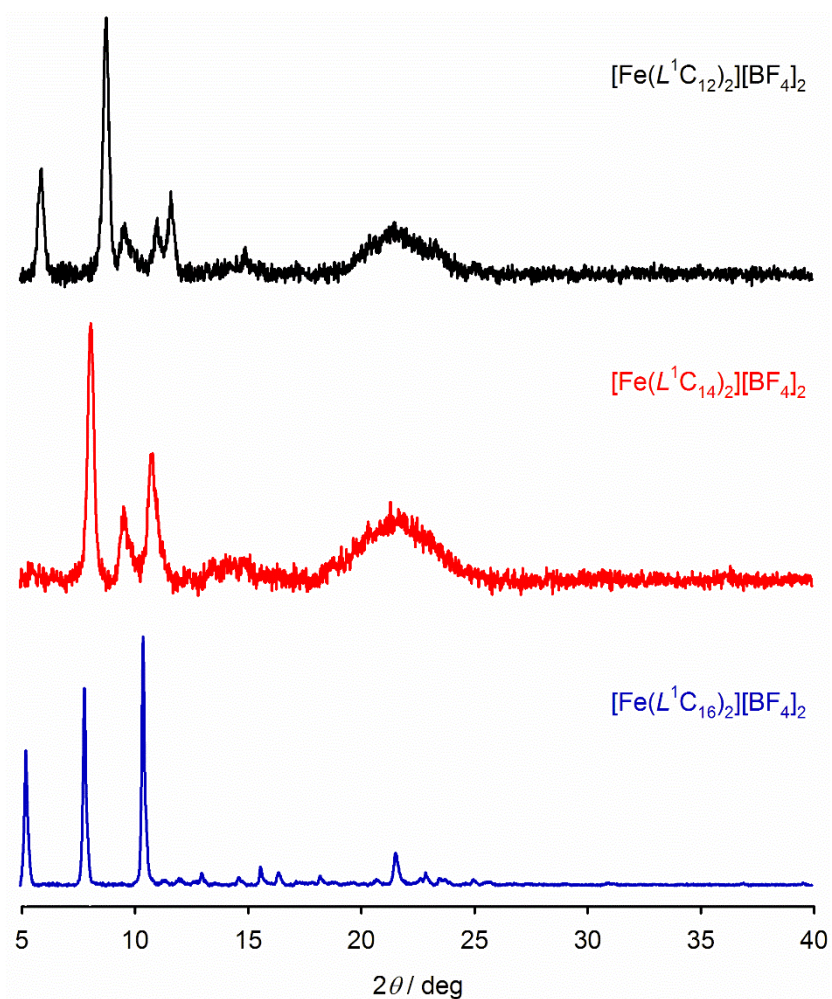
Figure S28 Room temperature X-ray powder diffraction data for the $[Fe(L^1C_n)_2][BF_4]_2$ series of complexes.

$[Fe(L^1C_{12})_2][BF_4]_2$ and $[Fe(L^1C_{14})_2][BF_4]_2$ appear isomorphous but poorly crystalline, with a strong amorphous hump near $2\theta = 22°$. Hence, these are clearly mixtures of crystalline and amorphous material.

The sample of $[Fe(L^1C_{16})_2][BF_4]_2$ has better crystallinity, and is isostructural with $[Fe(L^2C_{16})_2][BF_4]_2$ (Figure 2, main article and Figure S30).
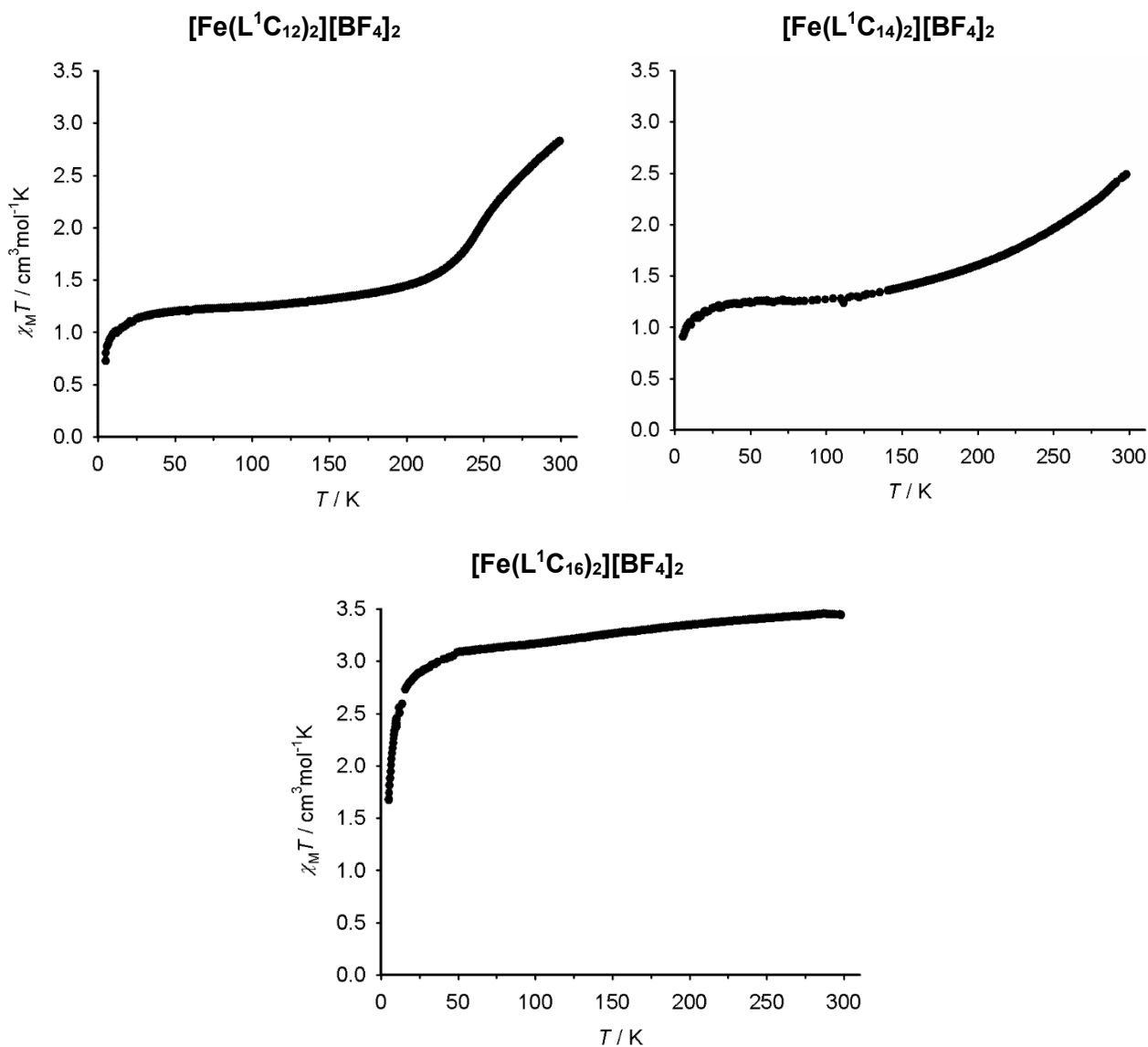
Figure S29 Magnetic susceptibility data for $[Fe(L^1C_n)_2][BF_4]_2$ (n = 12, 14, 16) at a scan rate of 5 K min^{-1}. All data were measured on a cooling temperature ramp.

The data for $[Fe(L^1C_{16})_2][BF_4]_2$ are the same as in Figure 3 of the main article.
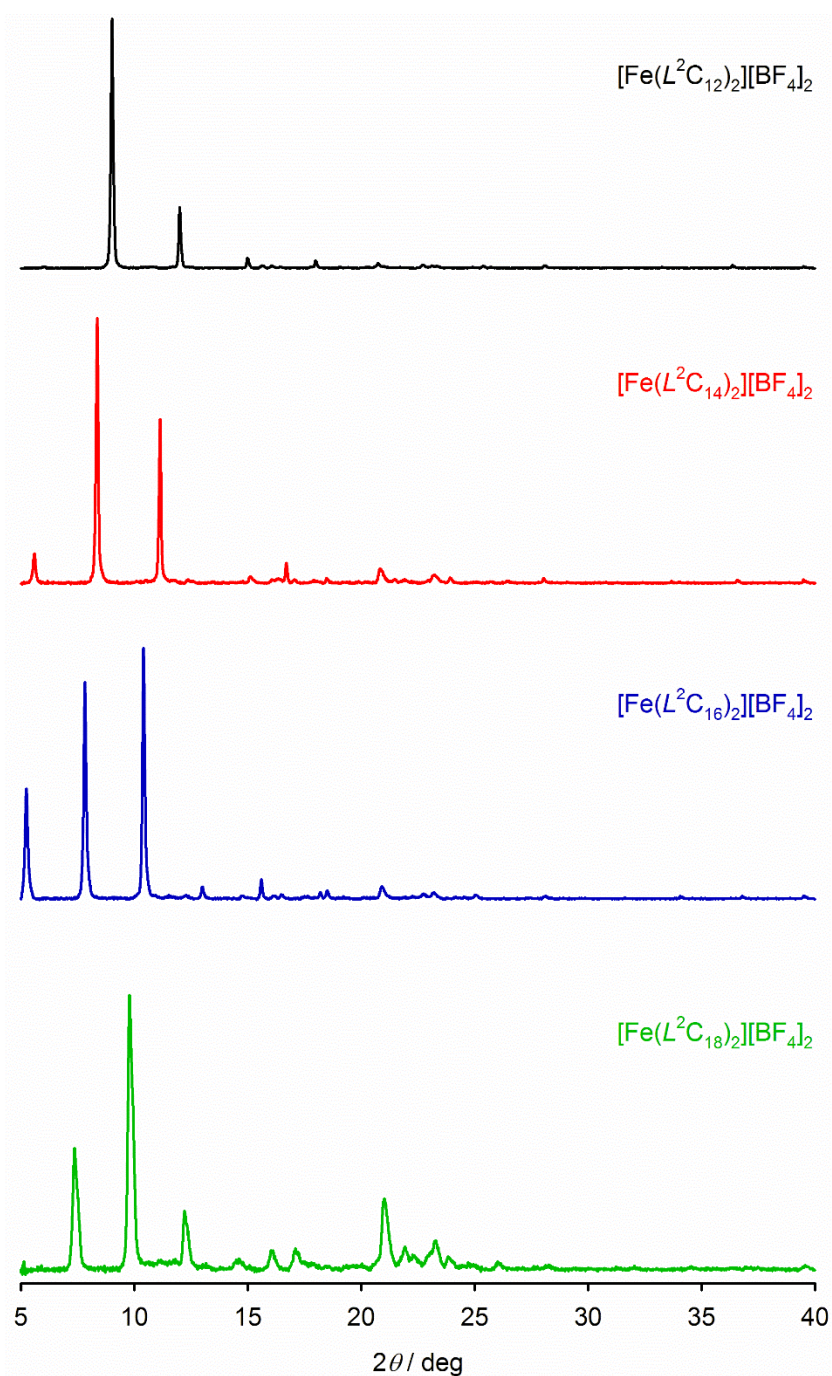
Figure S30 Room temperature X-ray powder diffraction data for the [Fe(L^{2}C$_n$)$_2$][BF$_4$]$_2$ series of complexes.

The similar form of these powder patterns implies these complexes are all isomorphous. That is consistent with the crystallographic data for [Fe(L^{2}C$_{12}$)$_2$][BF$_4$]$_2$, [Fe(L^{2}C$_{16}$)$_2$][BF$_4$]$_2$ and [Fe(L^{2}C$_{18}$)$_2$][BF$_4$]$_2$ (Figure S31).
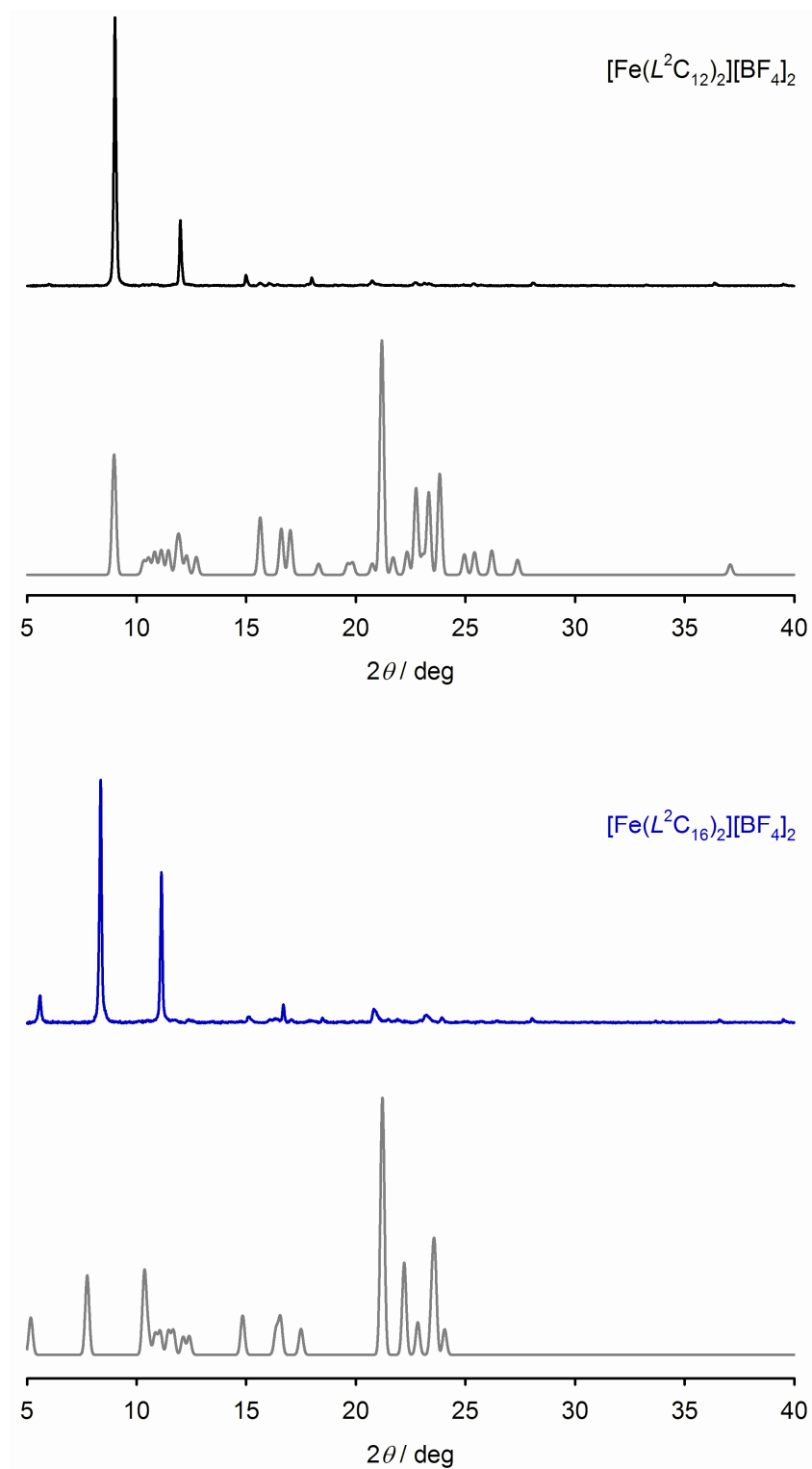
Figure S31 Measured (black or blue) and simulated (grey) X-ray powder diffraction data for the isostructural $[Fe(L^2C_n)_2][BF_4]_2$ complexes (Table S2).

These data are discussed at the foot of this Figure, on the next page.

$[Fe(L^2C_{18})_2][BF_4]_2$

2θ / deg
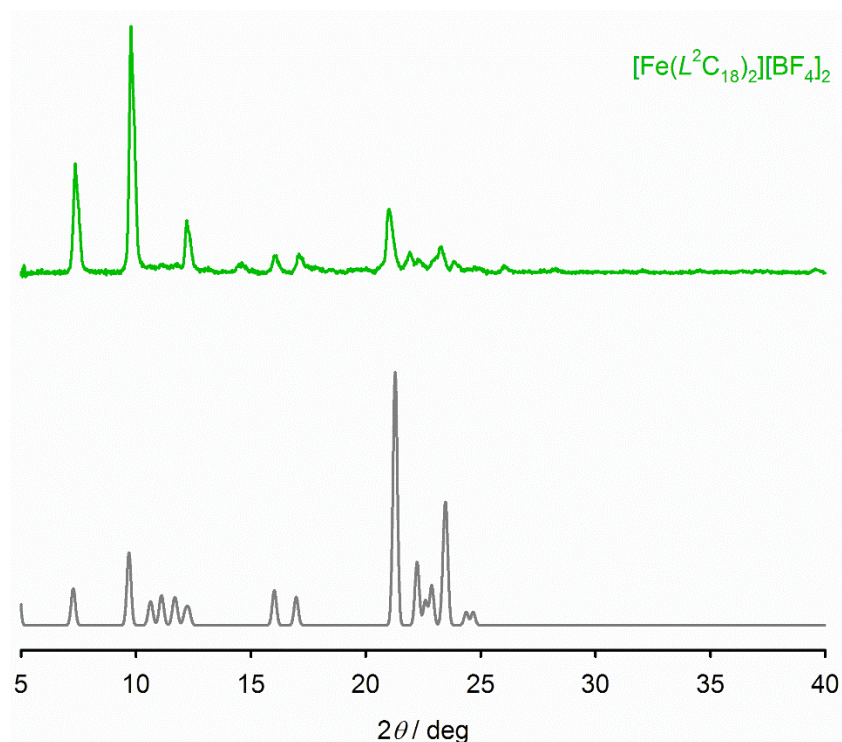
Figure S31 (continued).

The (002), (003) and (004) reflections are most strongly observed in all these powder patterns, especially for shorter L^2C_n chain lengths. Other expected reflections are either weak, or absent. Since the cation bilayers are oriented in the (001) plane, the correlated (00l) peaks are consistent with the highly lamellar crystal packing in these materials.[10]

The correspondence between the observed and simulated powder patterns for $[Fe(L^2C_{12})_2][BF_4]_2$ is interesting, since the bulk material contains lattice water by microanalysis, TGA and DSC whereas the single crystals do not. The flexibility of alkyl chains, which form the majority of the lattice, may allow water molecules to penetrate the structure without significantly changing its 3D ordering.[9]
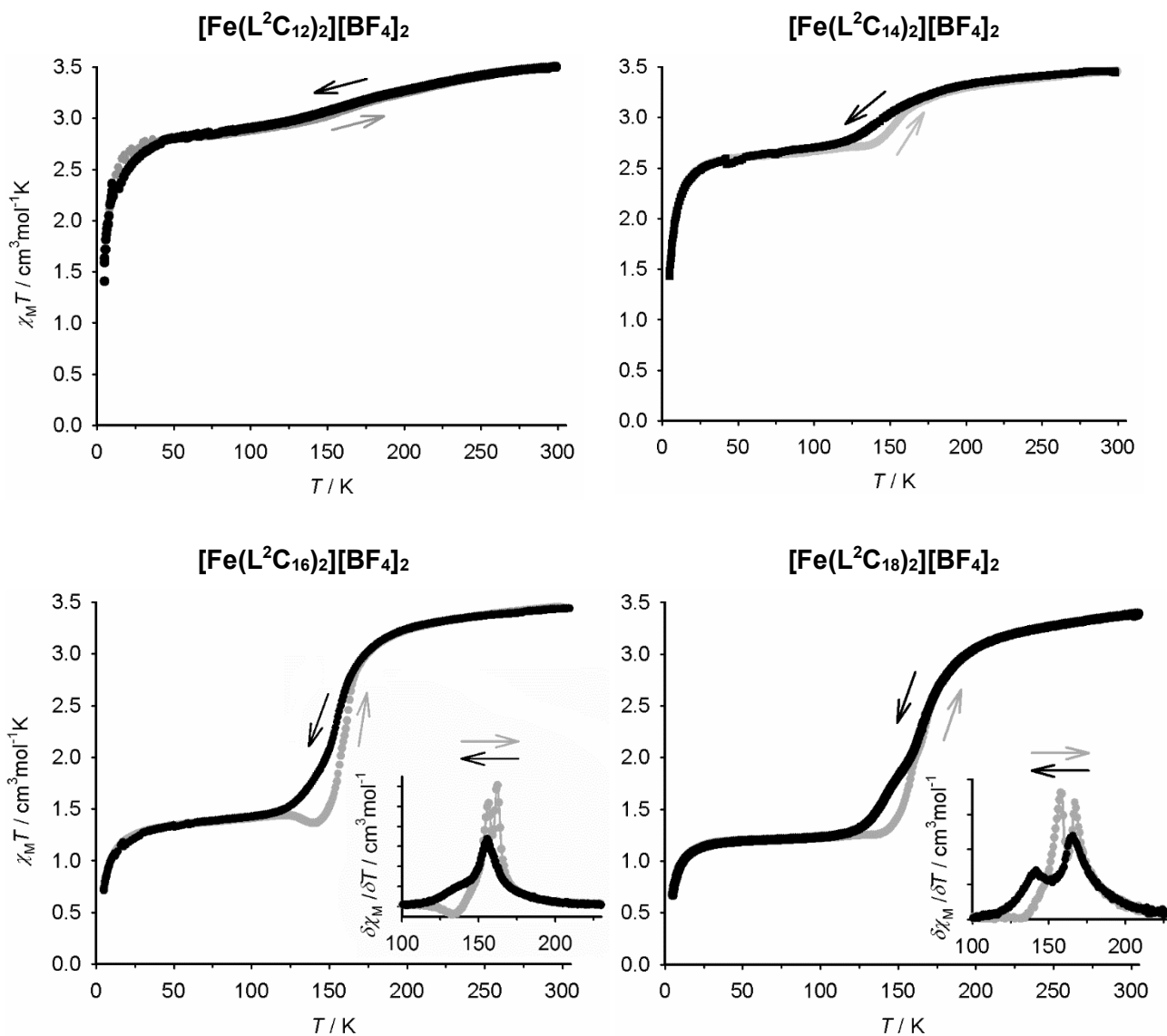
Figure S32 Magnetic susceptibility data for $[Fe(L^2C_n)_2][BF_4]_2$ (n = 12, 14, 16, 18) at a scan rate of 5 K min^{-1}. Data were measured on both cooling (black) and warming (grey) temperature ramps. The insets for show the first derivative of the plots for $[Fe(L^2C_{16})_2][BF_4]_2$ and $[Fe(L^2C_{18})_2][BF_4]_2$.

The data for $[Fe(L^2C_{16})_2][BF_4]_2$ are the same as in Figure 3 of the main article.
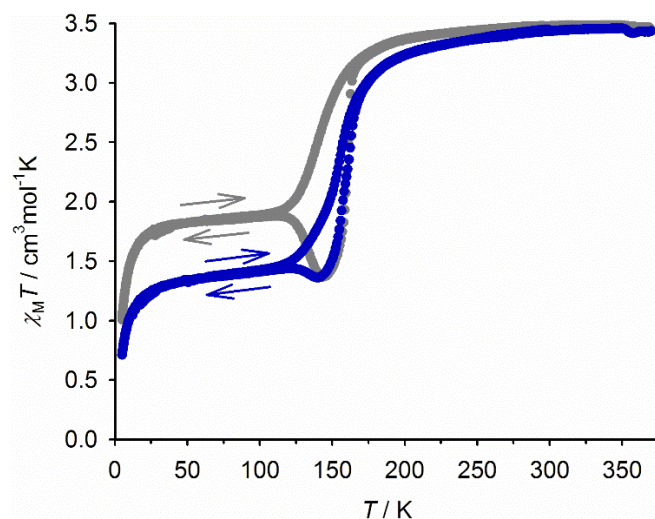
Figure S33 Magnetic susceptibility data for $[Fe(L^2C_{16})_2][BF_4]_2$ at scan rates of 5 K min^{-1} (blue) and 10 K min^{-1} (grey), on a 350→5→350 K temperature cycle. The blue data are the same as in Figure S32, and Figure 3 (main article).

The small decrease in $\chi_M T$ on warming, near 130 K, indicates relaxation of the sample to its thermodynamic spin state population at that temperature. The SCO becomes less complete, and the relaxation step is more pronounced, at the faster scan rate. This behaviour is characteristic of the kinetic trapping of a fraction of the sample in its high-spin form, upon cooling of the sample.[11]
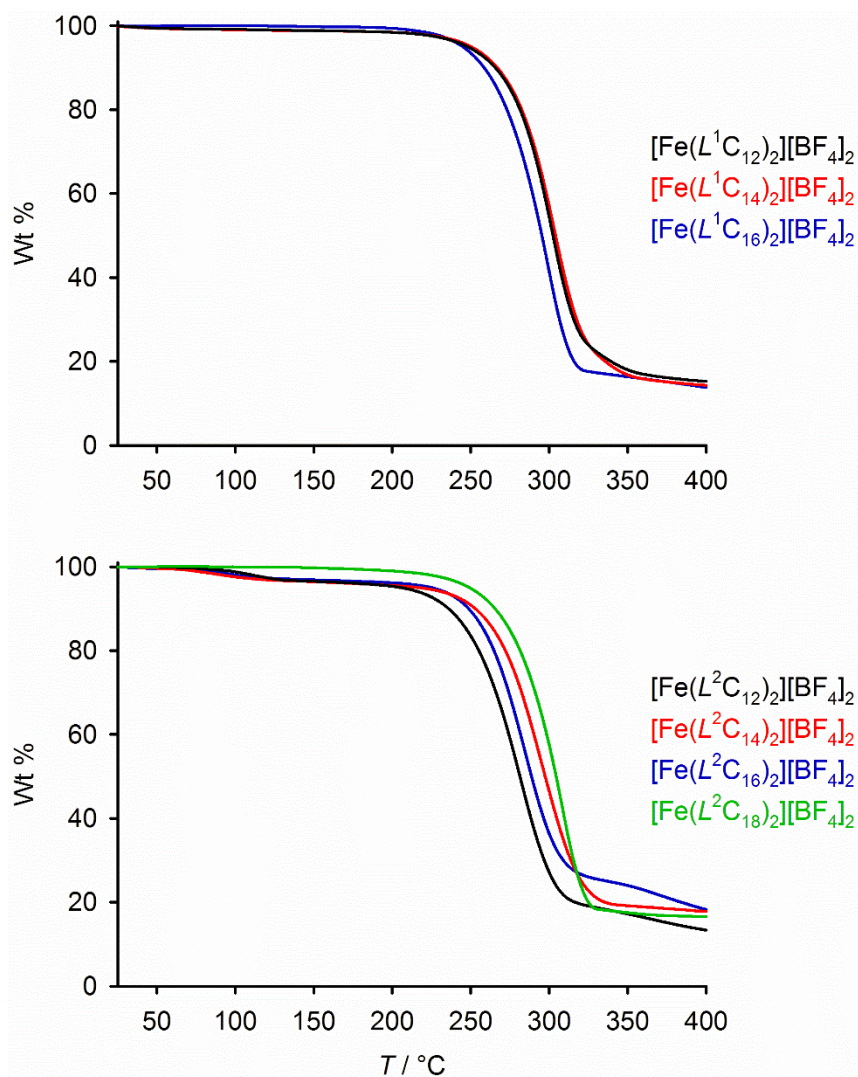
Figure S34 Thermogravimetric analysis (TGA) data for the $[Fe(L^1C_n)_2][BF_4]_2 \cdot x$solv (top) and $[Fe(L^2C_n)_2][BF_4]_2$ (bottom) series of complexes.

$[Fe(L^2C_n)_2][BF_4]_2$ (n = 12, 14 and 16) all show *ca* 3 % mass loss at 130 °C, which is equivalent to around 2 equiv H_2O. That contrasts with the crystal structure of $[Fe(L^2C_{12})_2][BF_4]_2$, which is anhydrous. However, it is broadly consistent with the elemental analyses of $[Fe(L^2C_{12})_2][BF_4]_2$ and $[Fe(L^2C_{14})_2][BF_4]_2$, which were both fit to a monohydrate formulation. The other complexes in this figure show ≤0.5 % mass loss at 100 °C, implying they don't contain significant lattice solvent.
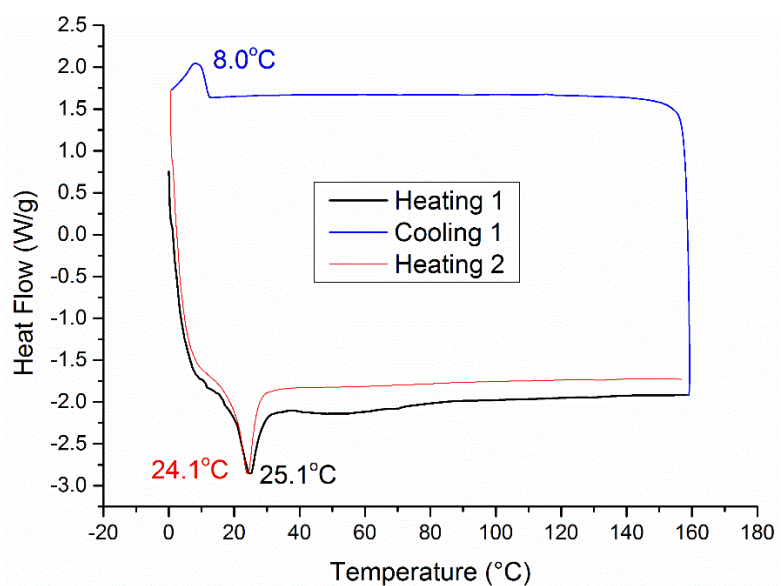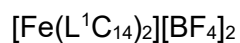
$[Fe(L^1C_{12})_2][BF_4]_2$

$[Fe(L^1C_{14})_2][BF_4]_2$

$[Fe(L^1C_{16})_2][BF_4]_2$
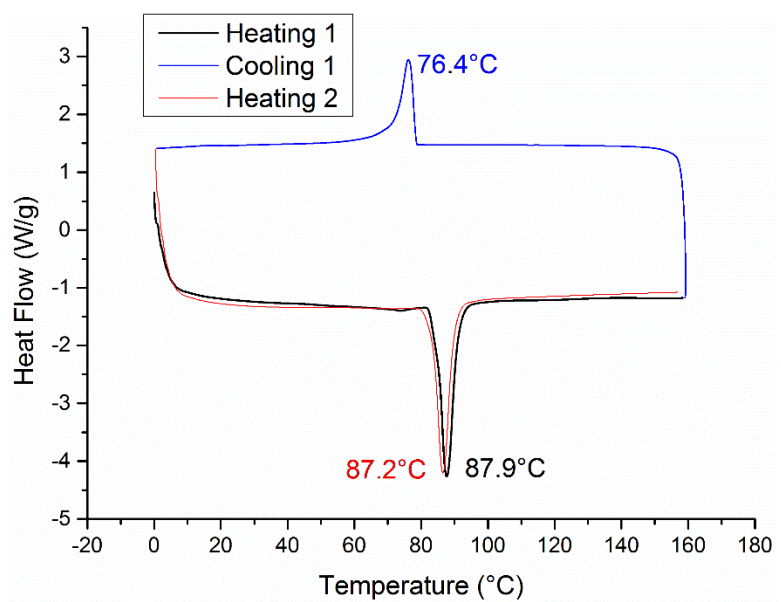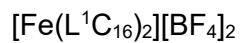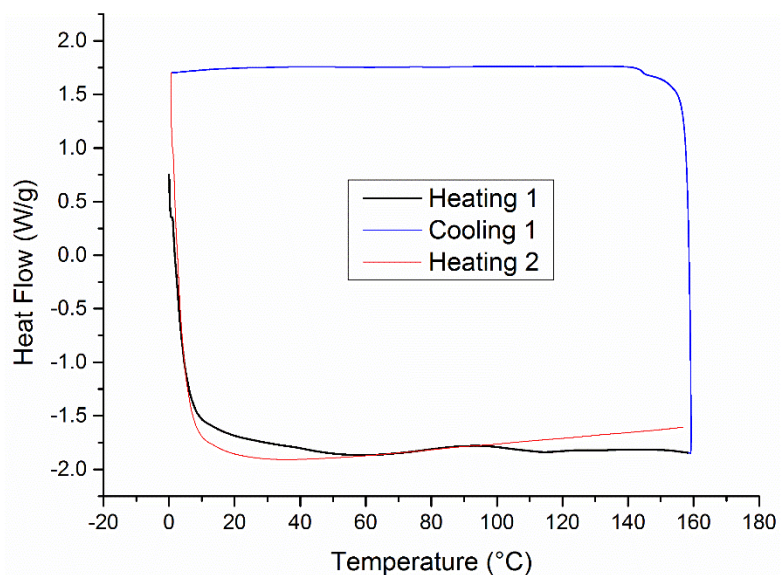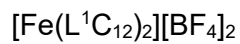
Figure S35 Differential Scanning Calorimetry (DSC) data for the $[Fe(L^1C_n)_2][BF_4]_2$ and $[Fe(L^2C_n)_2][BF_4]_2$ series of compounds (scan rate 10 K min^{-1}). These data are discussed at the bottom of the Figure.
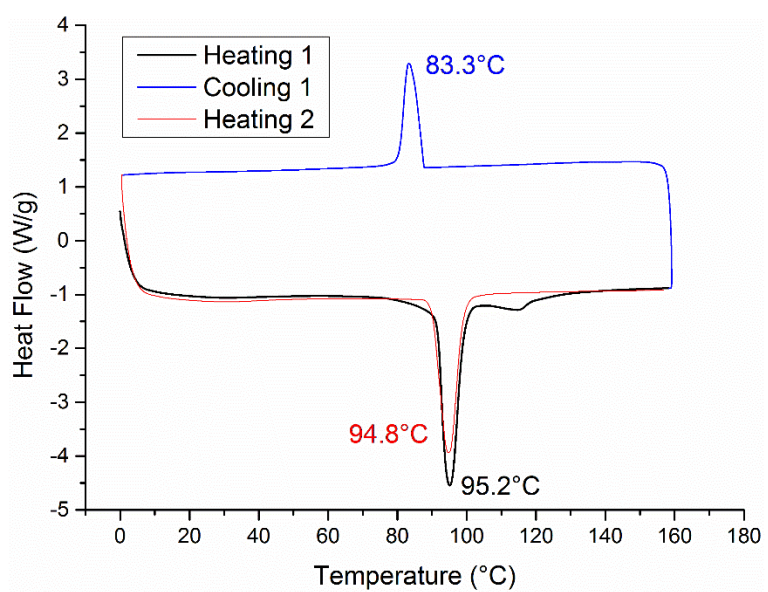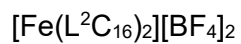
[Fe(L²C₁₂)₂][BF₄]₂·H₂O

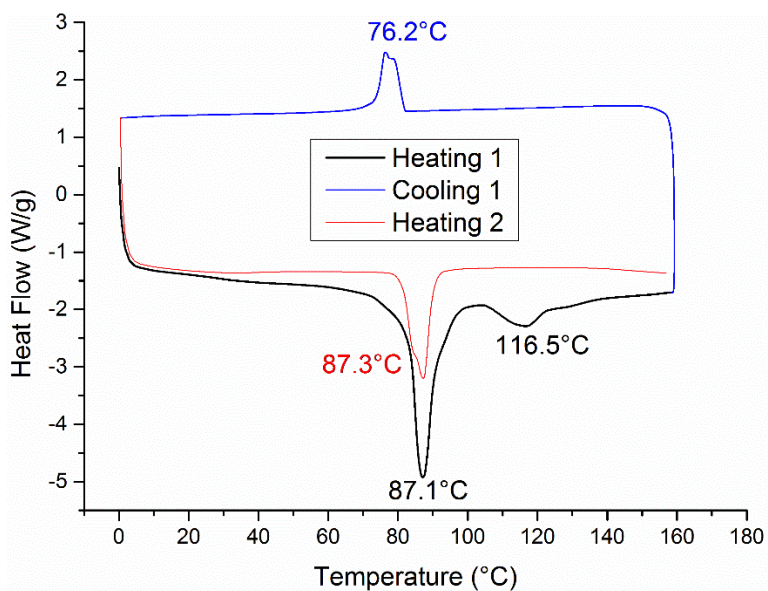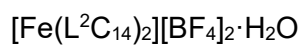[Fe(L²C₁₄)₂][BF₄]₂·H₂O

[Fe(L²C₁₆)₂][BF₄]₂

Figure S35 (continued)

$[Fe(L^2C_{18})_2][BF_4]_2$
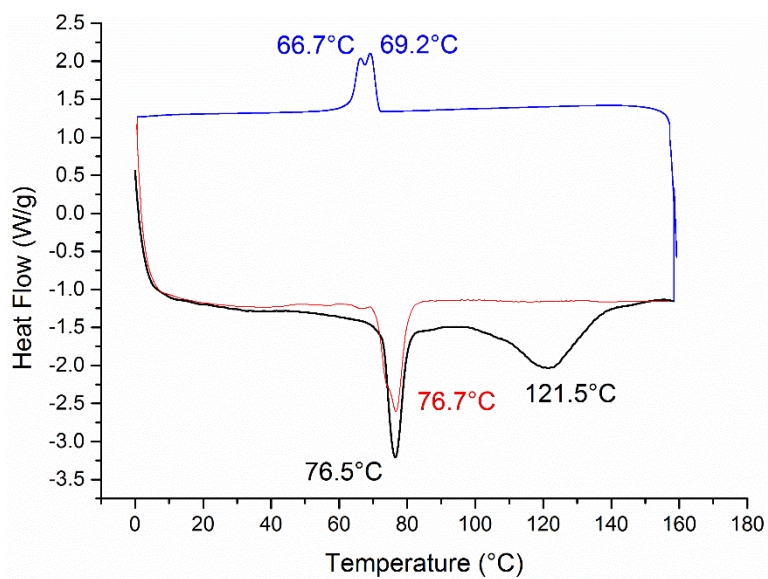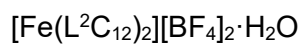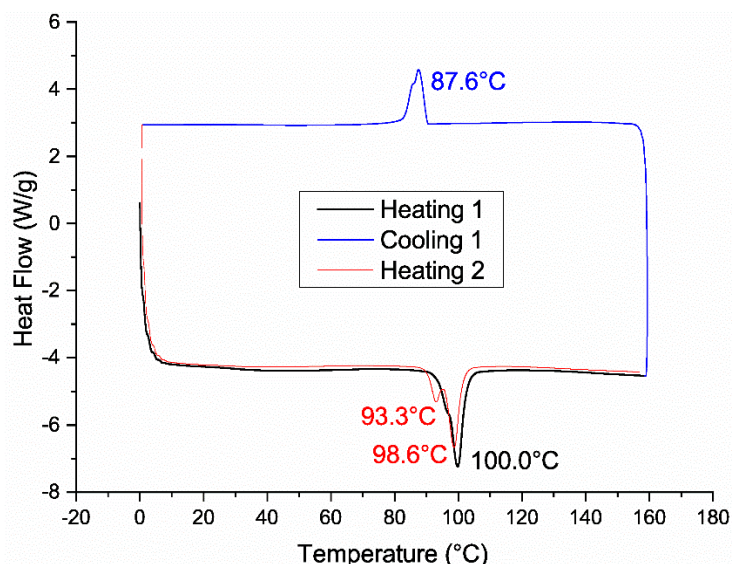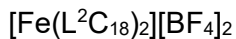
Figure S35 (continued)

$[Fe(L^1C_{12})_2][BF_4]_2$ and $[Fe(L^1C_{14})_2][BF_4]_2$ both exhibit a gradual, partial SCO equilibrium over this temperature range (Figure S28), which would not normally register in a DSC measurement. Thus the DSC of $[Fe(L^1C_{12})_2][BF_4]_2$ is featureless, and that of $[Fe(L^1C_{14})_2][BF_4]_2$ is almost the same with just one weak and reversible endotherm at room temperature. Since these samples are mixtures of poorly crystalline and amorphous material (Figure S28), the origin of that weak endotherm is unclear.

All the other compounds in the Figure (which are isomorphous by powder diffraction) show a much stronger reversible DSC feature, at a temperature between 77 and 100 °C; for the $[Fe(L^2C_n)_2][BF_4]_2$ series, the temperature increases consistently with increasing alkyl chain length n. This is not SCO-related, since the compounds are high-spin at these temperatures; it is also not a melting or mesophase transition, since the compounds remain solid on heating to 170 °C (443 K; Figure S36).

$[Fe(L^2C_{12})_2][BF_4]_2 \cdot H_2O$ and $[Fe(L^2C_{14})_2][BF_4]_2 \cdot H_2O$ show an additional broad feature near 120 °C, which is close to a 3 % mass loss observed in the TGA of those compounds Figure S34). That feature is therefore ascribed to the loss of lattice water from the samples.
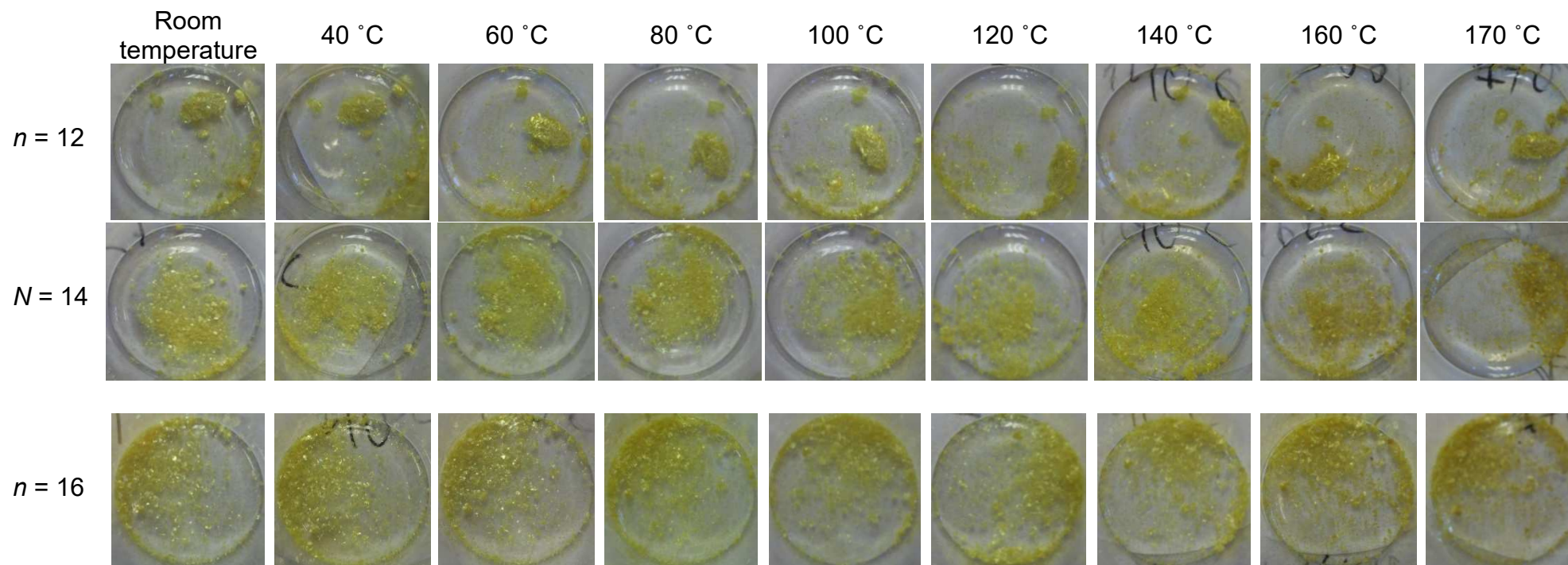
Figure S36 Samples of $[\text{Fe}(L^2\text{C}_n)_2][\text{BF}_4]_2$, photographed while being heated to different temperatures.

The compounds don't melt, change colour or obviously change their appearance on heating over this temperature range. Hence, the reversible endotherm at 77-95 °C in their DSC data does not correspond to a crystal-to-liquid-crystal transition, or to any spin-transition event. Most likely, it arises from a crystal-to-crystal phase change.

Figure S37 Magnetic data from [Fe(L^1C_{16})$_2$][BF$_4$]$_2$ (●) and [Fe(L^2C_{16})$_2$][BF$_4$]$_2$ (□) in CD$_3$CN solution. The lines show the best fits of the data to eq 1 and 2 (page S8).
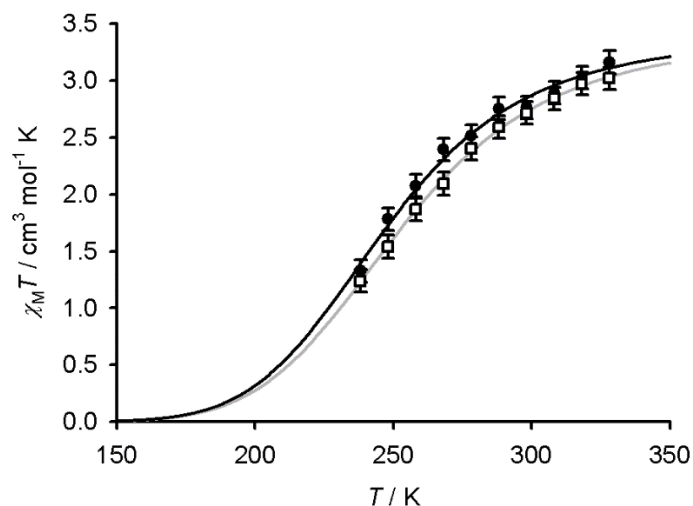
The fitted parameters for the SCO equilibria are:

For [Fe(L^1C_{16})$_2$][BF$_4$]$_2$ $T_{1/2}$ = 247 ±2 K; ΔH = −19.7 ±0.9 kJ mol^{-1}; ΔS = 80 ±4 J mol^{-1} K^{-1}.

For [Fe(L^2C_{16})$_2$][BF$_4$]$_2$ $T_{1/2}$ = 252.8 ±0.5 K; ΔH = −19.3 ±0.3 kJ mol^{-1}; ΔS = 76 ±1 J mol^{-1} K^{-1}.

These thermodynamic parameters are within the range expected for SCO by [Fe(bpp)$_2$]$^{2+}$ derivatives.[12] The larger errors for [Fe(L^1C_{16})$_2$][BF$_4$]$_2$ reflect that this compound is less soluble in the CD$_3$CN solvent, so a weaker solution was used for that measurement.

The slightly lower $T_{1/2}$ value shown by [Fe(L^1C_{16})$_2$][BF$_4$]$_2$ is consistent with the Hammett parameters of an akynyl (σ_M = +0.21) and an n-alkyl substituent (σ_M = −0.06).[13] Pyrazole C4 substituents with more negative σ_M values, which are more electron-donating, tend to increase $T_{1/2}$ in [Fe(bpp)$_2$]$^{2+}$ derivatives.[12]

Ref 12 implies a [Fe(bpp)$_2$]$^{2+}$ derivative with four alkynyl pyrazolyl substituents should exhibit $T_{1/2}$ *ca* 10 K lower than an analogue with four alkyl substituents. The 6 K difference between [Fe(L^1C_{16})$_2$][BF$_4$]$_2$ and [Fe(L^2C_{16})$_2$][BF$_4$]$_2$, which have only two of each substituent, is in line with the literature result.

References

1   S. Basak, Y. S. L. V. Narayana, M. Baumgarten, K. Müllen and R. Chandrasekar, *Macromolecules*, 2013, **46**, 362.

2   (a) L. Wang, N. Liu and B. Dai, *RSC Adv.*, 2015, **5**, 82097;
     (b) I. Galadzhun, I. Capel Berdiell, N. Shahid and M. A. Halcrow, *CrystEngComm*, 2019, **21**, 6330.

3   G. M. Sheldrick, *Acta Cryst. Sect. C.: Struct. Chem.*, 2015, **71**, 3.

4   L. J. Barbour, *J. Supramol. Chem.*, 2001, **1**, 189.

5   O. V. Dolomanov, L. J. Bourhis, R. J. Gildea, J. A. K. Howard and H. Puschmann, *J. Appl. Cryst.*, 2009, **42**, 339.

6   C. J. O'Connor, *Prog. Inorg. Chem.*, 1982, **29**, 203.

7   (a) D. F. Evans, *J. Chem. Soc.*, 1959, 2003;
     (b) E. M. Schubert, *J. Chem. Educ.*, 1992, **69**, 62.

8   B. García and J. C. Ortega, *J. Chem. Eng. Data*, 1988, **33**, 200.

9   I. Galadzhun, R. Kulmaczewski, O. Cespedes, M. Yamada, N. Yoshinari, T. Konno and M. A. Halcrow, *Inorg. Chem.*, 2018, **57**, 13761.

10   See eg
     (a) S. Barman, N. V. Venkataraman, S. Vasudevan and R. Seshadri, *J. Phys. Chem. B*, 2003, **107**, 1875;
     (b) H. Li, W. Bu, W. Qi and L. Wu, *J. Phys. Chem. B*, 2005, **109**, 21669;
     (c) P. N. Nelson and H. A. Ellis, *Dalton Trans.*, 2012, **41**, 2632;
     (d) G. Gbabode, M. Dohr, C. Niebel, J.-Y. Balandier, C. Ruzié, P. Négrier, D. Mondieig, Y. H. Geerts, R. Resel and M. Sferrazza, *ACS Appl. Mater. Interfaces*, 2014, **6**, 13413.

11   See eg
     (a) G. Ritter, E. König, W. Irler and H. A. Goodwin, *Inorg. Chem.*, 1978, **17**, 224;
     (b) V. A. Money, C. Carbonera, J. Elhaïk, M. A. Halcrow, J. A. K. Howard and J.-F. Létard, *Chem. Eur. J.*, 2007, **13**, 5503.
     (c) Y. Garcia, V. Ksenofontov, S. Mentior, M. Dirtu, C. Gieck, A. Bhatthacharjee and P. Gütlich, *Chem. Eur. J.*, 2008, **14**, 3745;
     (d) J.-F. Létard, S. Asthana, H. J. Shepherd, P. Guionneau, A. E. Goeta, N. Suemura, R. Ishikawa and S. Kaizaki, *Chem. Eur. J.*, 2012, **18**, 5924;
     (e) N. Paradis, G. Chastanet, F. Varret and J.-F. Létard *Eur. J. Inorg. Chem.* 2013, 968;
     (f) R. Kulmaczewski, E. Trzop, L. J. Kershaw Cook, E. Collet, G. Chastanet and M. A. Halcrow, *Chem. Commun.,* 2017, **53**, 13268.

12   L. J. Kershaw Cook, R. Kulmaczewski, R. Mohammed, S. Dudley, S. A. Barrett, M. A. Little, R. J. Deeth and M. A. Halcrow, *Angew. Chem. Int. Ed.*, 2016, **55**, 4327.

13   C. Hansch, A. Leo and R. W. Taft, *Chem. Rev.,* 1991, **91**, 165.